Research Paper

GEOSPHERE

GEOSPHERE, v. 17, no. 6

https://doi.org/10.1130/GES02409.1

11 figures; 1 table; 1 set of supplemental files

CORRESPONDENCE: azuza@unr.edu; avz5818@gmail.com

CITATION: Say, M.C., and Zuza, A.V., 2021, Heterogenous late Miocene extension in the northern Walker Lane (California-Nevada, USA) demonstrates vertically decoupled crustal extension: Geosphere, v. 17, no. 6, p. 1762–1785, https://doi.org/10.1130/GES02409.1.

Science Editor: Shanaka de Silva
Associate Editor: Todd LaMaskin

Received 29 January 2021
Revision received 3 May 2021
Accepted 14 July 2021

Published online 23 September 2021

Heterogenous late Miocene extension in the northern Walker Lane (California-Nevada, USA) demonstrates vertically decoupled crustal extension

Michael C. Say and Andrew V. Zuza

Nevada Bureau of Mines and Geology, University of Nevada, Reno, Nevada 89557, USA

ABSTRACT

The spatial distribution and kinematics of intracontinental deformation provide insight into the dominant mode of continental tectonics: rigid-body motion versus continuum flow. The discrete San Andreas fault defines the western North America plate boundary, but transtensional deformation is distributed hundreds of kilometers eastward across the Walker Lane–Basin and Range provinces. In particular, distributed Basin and Range extension has been encroaching westward onto the relatively stable Sierra Nevada block since the Miocene, but the timing and style of distributed deformation overprinting the stable Sierra Nevada crust remains poorly resolved. Here we bracket the timing, magnitude, and kinematics of overprinting Walker Lane and Basin and Range deformation in the Pine Nut Mountains, Nevada (USA), which are the westernmost structural and topographic expression of the Basin and Range, with new geologic mapping and $^{40}Ar/^{39}Ar$ geochronology. Structural mapping suggests that north-striking normal faults developed during the initiation of Basin and Range extension and were later reactivated as northeast-striking oblique-slip faults following the onset of Walker Lane transtensional deformation. Conformable volcanic and sedimentary rocks, with new ages spanning ca. 14.2 Ma to 6.8 Ma, were tilted 30°–36° northwest by east-dipping normal faults. This relationship demonstrates that dip-slip deformation initiated after ca. 6.8 Ma. A retrodeformed cross section across the range suggests that the range experienced 14% extension. Subsequently, Walker Lane transtension initiated, and clockwise rotation of the Carson domain may have been accommodated by northeast-striking left-slip faults. Our work better defines strain patterns at the western extent of the Basin and Range province across an approximately 150-km-long east-west transect that reveals domains of low strain (~15%) in the Carson Range–Pine Nut Mountains and Gillis Range surrounding high-magnitude extension (~150%–180%) in the Singatse and Wassuk Ranges. There is no evidence for irregular crustal thickness variations across this same transect—either in the Mesozoic, prior to extension, or today—which suggests that strain must be accommodated differently at decoupled crustal levels to result in smooth, homogenous crustal thickness values despite the significantly heterogeneous extensional evolution. This example across an ~150 km transect demonstrates that the use of upper-crust extension estimates to constrain pre-extension crustal thickness, assuming pure shear as commonly done for the Mesozoic Nevadaplano orogenic plateau, may not be reliable.

Andrew V. Zuza https://orcid.org/0000-0001-6130-5121

INTRODUCTION

Continental plate boundaries can be distributed and diffuse, with relative plate motion accommodated by wide zones (i.e., hundreds to thousands of kilometers) of deformation as observed in the San Andreas fault–Walker Lane–Basin and Range system of western North America or the Himalaya-Tibetan orogen (Atwater, 1970; Davis and Burchfiel, 1973; Molnar and Tapponnier, 1975; Thatcher, 1995; Flesch et al., 2000; Yin, 2010; Evans et al., 2016). Intraplate kinematics is described by either plate-like rigid-body motion separated by discrete faults (e.g., Luyendyk et al., 1980; Tapponnier et al., 1982; Weldon and Humphreys, 1986; Avouac and Tapponnier, 1993; Meade and Hager, 2005; Meade, 2007) or viscous flow with local high-strain zones within a deforming continuum (e.g., England and Houseman, 1986; Platt and Becker, 2010, 2013; Yin and Taylor, 2011; Haproff et al., 2018). An example of this problem is the spatial and temporal variation of Cenozoic extensional strain magnitudes and rates across the Basin and Range, western United States, in map view (e.g., Coney and Harms, 1984; McQuarrie and Wernicke, 2005; Long, 2019) that conflict with apparently well-distributed finite strain across the Great Basin, as shown by its uniform crustal thickness (e.g., Allmendinger et al., 1983; Gilbert, 2012). To explain this observation, it has been proposed that flow or influx of a low-viscosity lower crust smoothed out topography and Moho-depth variations (e.g., Gans, 1987; Bird, 1991; Kruse et al., 1991; McKenzie et al., 2000). This requires decoupling of the upper and lower crust, such that extensional strain recorded in the geologic record at Earth's surface does not reflect processes in the lower crust. Despite this kinematic requirement, models of the pre-extensional thickness of the Great Basin commonly rely on using upper-crust extensional magnitudes (e.g., McQuarrie and Wernicke, 2005) to restore crustal thickness of the inferred Nevadaplano orogenic plateau (DeCelles, 2004), assuming vertically coherent pure-shear extension of a crustal column (e.g., Coney and Harms, 1984; Best et al., 2009; Long, 2019; Bahadori and Holt, 2019).

To address the above issues, we conducted a focused study of the western Basin and Range

extensional province at ~39°N latitude, where extension has encroached westward onto the relatively stable rigid Sierra Nevada block since the middle Miocene (Dilles and Gans, 1995; Henry and Perkins, 2001; Surpless et al., 2002) (Fig. 1). Here, crustal extension estimates are extremely variable, with the Yerington district (i.e., Singatse Range) classically interpreted to reflect high-magnitude extension of >150% (e.g., Proffett, 1977), whereas the eastern Sierra Nevada–Carson Range is interpreted to have been extended <20% (e.g., Stockli, 1999; Surpless et al., 2002; Long, 2019) (Fig. 1). Despite these drastically different extensional strain magnitudes, present-day crustal thickness is similar across these regions and the Moho is relatively flat (e.g., Allmendinger et al., 1983; Surpless et al., 2002; Gilbert, 2012). There is also no evidence that Mesozoic crustal thickness values in this region were dissimilar—probably >60–70 km as part of the Sierra Nevada arc and immediate backarc (e.g., Profeta et al., 2015; Cao and Paterson, 2016)—and therefore efficient three-dimensional strain partitioning is required to distribute high and low magnitudes of extension. The spatial extent of this strain distribution is unclear, but the bulk extensional process must have homogenously thinned the Mesozoic crust from ~60 km to ~35 km today.

Furthermore, the Sierra Nevada–Basin and Range transitional boundary is overprinted by, or kinematically linked with, strike-slip shear associated with the progressive development of the Walker Lane (Moore and Archbold, 1969; Trexler et al., 2000; Henry and Perkins, 2001; Faulds et al., 2005; Sturmer and Faulds, 2018) (Fig. 1). Presently, ~15%–25% of Pacific–North American relative plate motion is accommodated east of the rigid Sierra Nevada block in the Walker Lane and Eastern California shear zone (Thatcher et al., 1999; Dixon et al., 2000; Svarc et al., 2002; Bennett et al., 2003; Hammond and Thatcher, 2004; Hammond et al., 2009). Therefore, the integrated relationship between the undeformed Sierra Nevada and deforming Walker Lane–Basin and Range provinces, both inboard of the San Andreas plate boundary, impacts our understanding of intracontinental tectonics and strain partitioning.

We focused on an ~150-km-long transect across the Carson domain of the northern Walker Lane that included, from west to east, the Sierra Nevada–Carson Range, Pine Nut Mountains, Singatse Range, Wassuk Range, and Gillis Range (Fig. 1). Our research goal was to provide a high-resolution kinematic evolution model of extension and transtension along this transect to investigate how strongly contrasting upper-crustal strain magnitudes can thin the crust homogenously. This study provides new constraints on the magnitude and timing of extension across the northern Pine Nut Mountains, building on mapping presented in Say and Zuza (2020). The study area involved faulted Miocene volcanic rocks that allowed us to simultaneously estimate the magnitude and timing of extension for comparison with other published data sets. We provide nine new $^{40}Ar/^{39}Ar$ ages from deformed volcanic stratigraphy, in addition to two previous ages from Say and Zuza (2020). Our work documents a Miocene extensional lull that reflects complex plate-boundary processes. Integration of our extensional strain estimates with regional data sets confirms heterogenous strain across this traverse that we argue must be accommodated via vertically decoupled crustal extension.

GEOLOGIC SETTING AND STRUCTURAL FRAMEWORK

Our new observations are from the northern Pine Nut Mountains, which we integrated with data from the surrounding ranges (Fig. 1B). Figure 2 summarizes the geologic history of this region in block models. The bedrock geology is related to the Mesozoic subduction history of the eastern Pacific realm (Dickinson, 2004; DeCelles, 2004). East-dipping subduction started in the Late Triassic–Early Jurassic along the western margin of the North America continent, which led to arc magmatism and volcanism (e.g., Schweickert, 1978; Saleeby et al., 2015; Levy et al., 2021). Locally, the Gardnerville Formation, composed of metasedimentary and metavolcanic rocks, was deposited during the earlier stages of subduction and magmatism, and these rocks have been biostratigraphically dated to late Norian (227–208 Ma) to late Toarcian (182–174 Ma) (Noble, 1962; Stewart, 1997). Recent U-Pb zircon dating confirms this assignment (i.e., ca. 177 Ma; Say and Zuza, 2020).

Subduction and arc magmatism persisted in the Middle Jurassic to Late Cretaceous (DeCelles, 2004; Dickinson, 2004; DeCelles and Graham, 2015; Yonkee and Weil, 2015), generating Mesozoic plutons (e.g., the Yerington batholith, Shamrock batholith, Sunrise Pass pluton; Dilles and Wright, 1988; Stewart, 1999) (Fig. 2A). Coupled magmatism and intra-arc and retroarc shortening led to crustal thickening as part of an inferred high-elevation orogenic plateau, termed the Nevadaplano, which was located within the hinterland of the Sevier foreland thrust belt observed in central Utah (DeCelles, 2004; Dickinson, 2006; Ernst, 2010; Henry et al., 2012). Growth of this plateau probably started in the Middle–Late Jurassic (Wyld, 2002; Miller and Hoisch, 1995; Zuza et al., 2020a, 2021), and crustal shortening, magmatism, and thickening peaked in the Late Cretaceous (Coney and Reynolds, 1977; Dickinson and Snyder, 1978; Humphreys et al., 2003; DeCelles and Graham, 2015; Yonkee and Weil, 2015). Estimates for the thickness of this plateau are derived from structural restorations, geochemical proxies, and inferences from stable isotope paleoaltimetry, which all suggest that much of the Nevadaplano was ≥60 km thick (e.g., Coney and Harms, 1984; Chapman et al., 2015; Cassel et al., 2009, 2014). Mass-balance calculations from the Sierra Nevada magmatic arc also suggest that the crust was >60 km thick (Cao and Paterson, 2016). West-east spatial variations in crustal thickness, including inferences of thickened crustal welts near the present-day California-Nevada and Nevada-Utah borders, are poorly resolved and are based primarily on structural restorations of localized high-magnitude extension (Coney and Harms, 1984; Long, 2019; Bahadori and Holt, 2019).

Observations of throughgoing paleovalleys, which would have incised across elevated topography (DeCelles, 2004; Dickinson, 2006; Ernst, 2010; Henry et al., 2012) (Fig. 2A), provide evidence for Cretaceous to early-to-middle Cenozoic persistence of the inferred Nevadaplano. In particular, Eocene (ca. 50–46 Ma) to late Oligocene (ca. 23 Ma) paleovalleys drained westward across the western Nevadaplano and Sierra Nevada, which resulted in

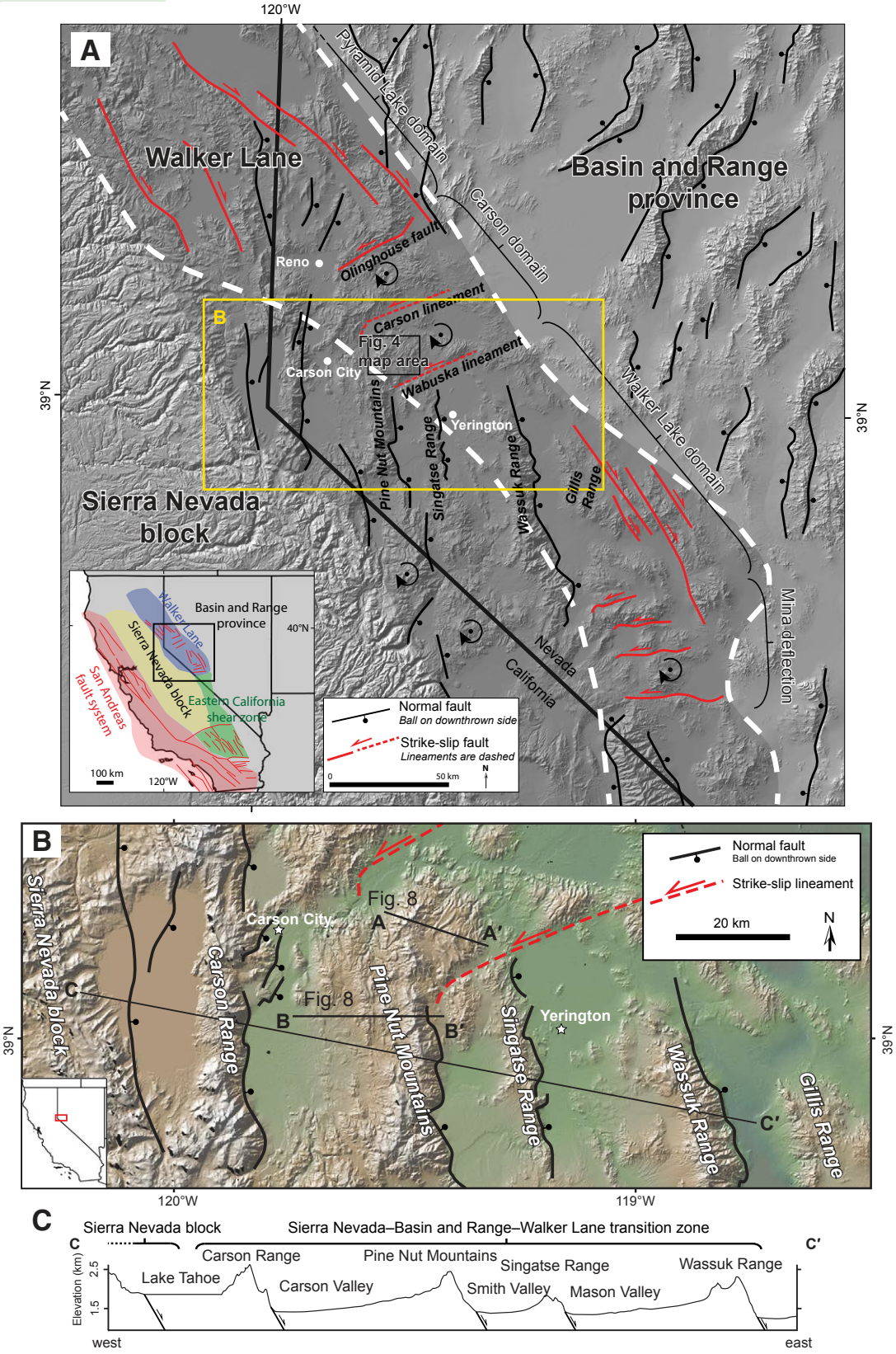

Figure 1. Regional topographic and fault maps across the northern Walker Lane of western Nevada, USA. (A) Map of major faults in the Walker Lane and Basin and Range deformational provinces (normal faults in black; strike-slip faults in red; rotation arrows show clockwise rotation of structural blocks in the Walker Lane). Shaded gray outline depicts the Walker Lane boundary defined by Wesnousky (2005a), and white dashed outline is the Walker Lane boundary defined by Faulds and Henry (2008). Basemap created using GeoMapApp (Ryan et al., 2009). Inset map displays major fault systems in the western United States including the rigid Sierra Nevada block. Figure adapted from Cashman and Fontaine (2000), Li et al. (2017), Sturmer and Faulds (2018), and Zuza and Carlson (2018). Yellow box shows the location of B. (B) Overview map of major faults and ranges near along the Sierra Nevada–Walker Lane–Basin and Range transition zone and the Pine Nut Mountains cross sections in Figure 8 are shown as A-A′ (this study) and B-B′ (Long, 2019). Cross section C-C′ is shown in panel C of this figure. (C) Elevation profile of the ranges and basins to the east of the Sierra Nevada block.

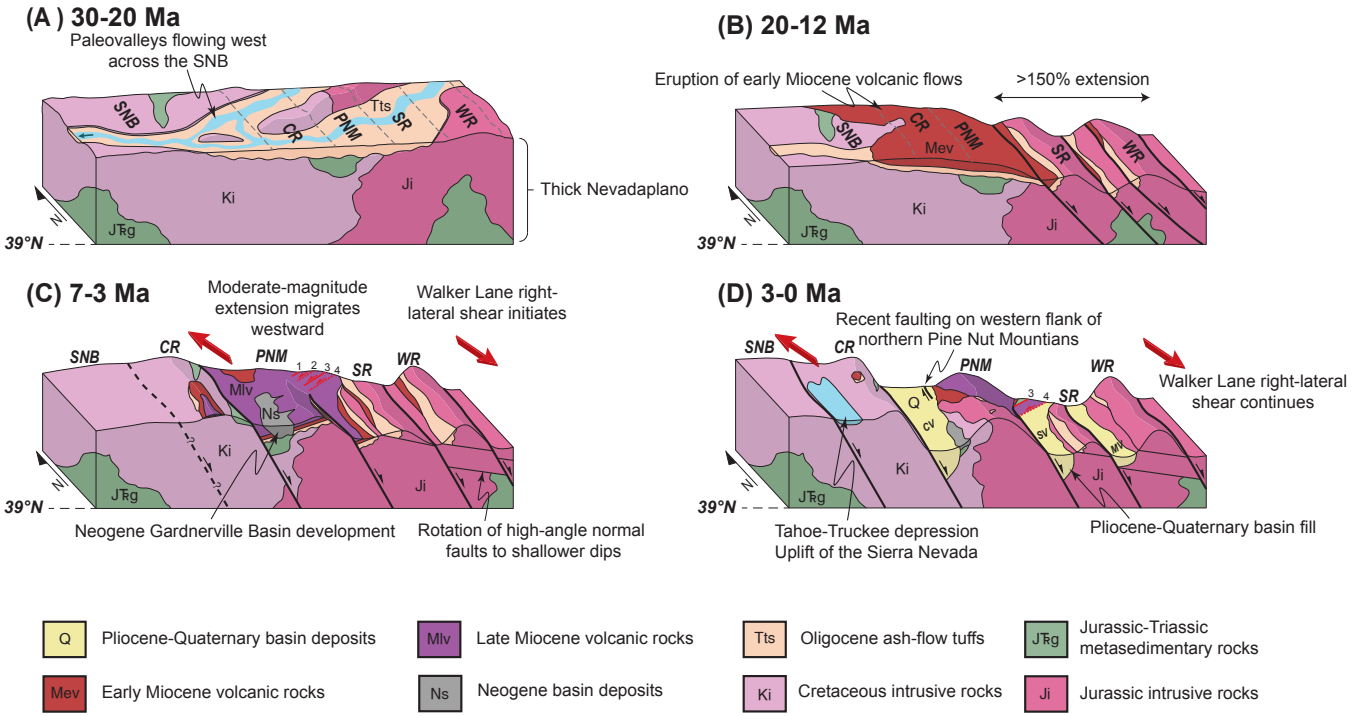

Figure 2. Structural block model for the evolution of the Sierra Nevada–Walker Lane–Basin and Range transition zone at the approximate latitude of 39°N. (A) Pre-extensional setting of the Nevadaplano. Paleovalleys periodically filled with Oligocene ash-flow tuffs. (B) High-magnitude extension (>150% extension) on the eastern edge of the transition zone begins ca. 15 Ma. (C) Extension encroaches westward on the Sierra Nevada block with later initiation of Walker Lane right-lateral shear. (D) Extension and Walker Lane right-lateral shear migrates further west into the Sierra Nevada block ca. 3 Ma and deformation continues to the present day, forming the modern basins and range topography in the transition zone. Mountains and range names: SNB—Sierra Nevada block; CR—Carson Range; PNM—Pine Nut Mountains; SR—Singatse Range; WR—Wassuk Range. Left-slip faults and lineaments: 1—Olinghouse fault; 2—Carson lineament; 3—Bull Canyon fault; 4—Wabuska lineament. CV—Carson Valley; SV—Smith Valley; MV—Mason Valley.

the deposition of well-characterized ash-flow tuffs that infilled these valleys (Henry, 2008; Henry and Faulds, 2010; Henry et al., 2012) (e.g., Fig. 2A). Oligocene ash-flow tuffs and sedimentary rocks were deposited over Mesozoic plutons and metamorphic rocks in the southern Pine Nut Mountains (Noble, 1962; Moore and Archbold, 1969) and surrounding ranges (Castor, 1972; Proffett and Dilles, 1984; Dilles and Gans, 1995; Surpless et al., 2002).

A widespread ignimbrite flareup (36–18 Ma), intermediate-composition volcanism of the Ancestral Cascade arc (22–5 Ma), and bimodal volcanism related to Basin and Range extension (13 Ma to present; Stewart, 1988; Best et al., 1989, 2013; Christiansen et al., 1992; Faulds et al., 2005; Cousens et al., 2008; du Bray and John, 2011) affected western Nevada (Fig. 2B). The study area consists of an intermediate to felsic suite of volcanic flows and shallow intrusions that are representative of Ancestral Cascade arc magmatism (e.g., Cousens et al., 2008; Say and Zuza, 2020). Starting ca. 16–15 Ma, Miocene volcanic flows blanketed much of the area (Dilles and Gans, 1995; Stewart, 1999). Late Cenozoic arc volcanism in western Nevada slowed and arc cessation migrated northwestward following the Miocene northwestward migration of the Mendocino triple junction, which is currently west of the study area (Atwater and Stock, 1998; Faulds et al., 2005).

The thickened Nevadaplano collapsed during Cenozoic extension (e.g., Coney and Harms, 1984; Colgan and Henry, 2009; Henry et al., 2011). The exact drivers of regional extension are highly debated, and end-member models can be grouped as (1) gravitational collapse of the thickened Nevadaplano crust or (2) changes in plate-boundary stresses as relative plate motion reorganized, or a combination of these mechanisms (e.g., Sonder and Jones, 1999; Colgan and Henry, 2009). Regardless of extensional

mechanism, present-day crustal thickness across much of the Great Basin is ~35 km (Gilbert, 2012), and thus, crustal thickness was roughly cut in half from that of the Mesozoic orogenic plateau to today. Plate reconstructions demonstrate that the westward propagation of Basin and Range extension and inception of the Walker Lane coincides with the transition of the Pacific–North American convergent plate boundary to a right-lateral transform boundary, with increased relative plate motion and changing plate convergence directions from west-northwest to north-northwest at ca. 12 Ma (Atwater and Stock, 1998; Faulds and Henry, 2008; Cashman et al., 2009; Busby, 2013; DeMets and Merkouriev, 2016; Lee et al., 2020).

Extension in western Nevada at ~39°N latitude varied temporally and spatially. Extension isolated ranges (Figs. 1, 2B, and 2C) of predominately Sierran granitic bedrock from the main belt of the northwest-trending Sierra Nevada (Surpless et al., 2002; Unruh et al., 2003).The main phase of high-magnitude extension initiated around Yerington, Nevada, in the Wassuk and Singatse Ranges ca. 15–14 Ma (Dilles and Gans, 1995; Stockli et al., 2002; Surpless et al., 2002). However, Dilles and Gans (1995) argued for an early phase of normal and strike-slip faulting in the Yerington area—i.e., Singatse and Wassuk Ranges (Fig. 1)—from ca. 26 to 22 Ma. Normal faulting on closely spaced (1–2 km), east-dipping, north-striking high-angle faults that progressively rotated to shallower dips accommodated >150% extension over a relatively short time span from ca. 15 to 12.5 Ma (Proffett, 1977; Dilles and Gans, 1995). To the west, the style and magnitude of deformation drastically change to low-magnitude extension accommodated via high-angle normal faulting and minor range tilting (Surpless et al., 2002; Cashman et al., 2009; Long, 2019). Researchers have debated whether extension in the western Basin and Range resulted from westward-propagating Basin and Range extension (Surpless et al., 2002) or Walker Lane transtension (Cashman et al., 2009; Wesnousky, 2005b). The basis for these arguments deals with the timing of Walker Lane deformation and whether Basin and Range extension propagated west into the Sierra Nevada block.

In the late Miocene, Walker Lane right-lateral shear overprinted earlier extension (e.g., Faulds and Henry, 2008; Sturmer and Faulds, 2018). Walker Lane shear is variably expressed as northwest-striking right-slip faults and northeast-striking left-slip faults (e.g., Faulds and Henry, 2008). In the northern Walker Lane, there are three distinct domains: the Pyramid Lake domain in the north, central Carson domain, and the southern Walker Lake domain (Fig. 1; Wesnousky, 2005a; Faulds and Henry, 2008). The northern Walker Lane region accommodates ~10 mm yr^{-1} of right-lateral shear today as constrained via geodesy (Kreemer et al., 2009; Bormann et al., 2016). The Carson domain consists of three parallel east-northeast–striking left-slip faults or major lineaments (i.e., the Olinghouse fault, Carson lineament, and Wabuska lineament), whereas the Pyramid Lake and Walker Lake domains consist of northwest-striking right-slip faults (Fig. 1). The left-slip faults in the Carson domain, orthogonal to regional right-lateral shear, accommodate vertical-axis clockwise rotation of relatively rigid blocks (Fig. 3; Cashman and Fontaine, 2000; Li et al., 2017; Sturmer and Faulds, 2018; Say and Zuza, 2020). These primary faults in the Carson domain have estimated slip rates of ~1 mm yr^{-1} or less (Li et al., 2017). The initiation of Walker Lane deformation in the Carson domain is loosely constrained to 8–5 Ma (Faulds et al., 2005; Sturmer and Faulds, 2018).

Exhumation related to extension or transtension propagated westward from the Singatse Range toward the Pine Nut Mountains and Carson Range by ca. 11–3 Ma (Figs. 2B and 2C; Dilles and Gans, 1995; Henry and Perkins, 2001; Stockli et al., 2002; Surpless et al., 2002). Surpless et al. (2002) conducted apatite fission-track (AFT) analyses across a Cretaceous granodiorite-granite in the central Pine Nut Mountains that suggest exhumation-related cooling ca. 10–5 Ma. However, this age signal is not precise because it is constrained by AFT track-length modeling. High-angle, east-dipping normal faulting reinitiated in the Wassuk and Singatse Ranges ca. 4 Ma (Fig. 2C; Stockli et al., 2002).

From 3 Ma to present, extensional and transtensional deformation in the Sierra Nevada–Basin and Range–Walker Lane transition zone has migrated further west to form the Tahoe-Truckee depression, as well as the Verdi-Boca Basin to the north (Fig. 2D; Henry and Perkins, 2001; Cashman et al., 2009). During this time, extension has led to the uplift of the Carson Range and Sierra Nevada (Henry and Perkins, 2001; Surpless et al., 2002; Trexler et al., 2012). Apatite helium dating (AHe) and the exhumation of an AHe partial retention zone across the Carson Range suggests initiation of normal-fault related exhumation at 4 ± 3 Ma (Stockli, 1999). Pliocene–Quaternary basin fill has continued to develop in the range-bounded basins (Fig. 2D).

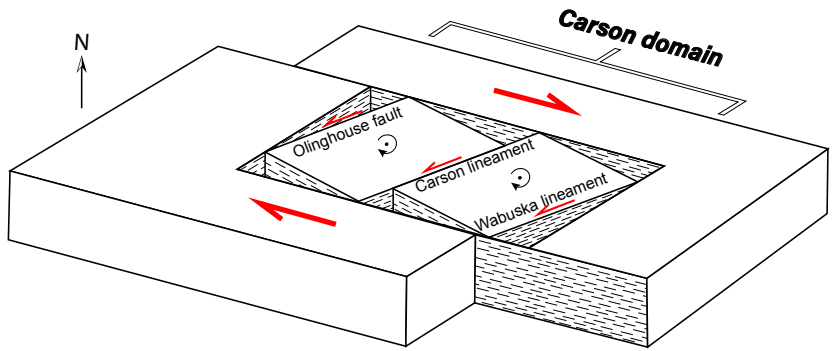

Figure 3. Schematic clockwise block rotation of the Carson domain, after the style of Oldow et al. (1994). Northwest-trending right-lateral shear of the Walker lane is accommodated in the Carson domain by clockwise rotation of structural blocks via orthogonal left-slip faults. Figure modified from Nagorsen-Rinke et al. (2013).

Presently, normal and strike-slip oblique faulting continues in the eastern portion of the transition zone, but no strike-slip or oblique structures have currently been identified west of the northern Pine Nut Mountains in Carson Valley (Fig. 2D). Geodesy demonstrates that the Sierra Nevada block is moving to the northwest relative to the Basin and Range (Kreemer et al., 2009), which implies some lateral motion in this region that is poorly resolved by geologic investigations (e.g., Pierce et al., 2021).

NEW OBSERVATIONS FROM THE PINE NUT MOUNTAINS

New observations are based on new 1:24,000-scale geologic mapping in the Pine Nut Mountains (Fig. 4), new argon dating, and structural observations and are integrated with published observations and data sets from surrounding ranges. The mapping expanded on the published Carson City 30′ × 60′ quadrangle (1:100,000 scale; Stewart, 1999) and local geologic maps of the Como Mining District (Russell, 1981; Vikre and McKee, 1994). Mapping was completed using satellite imagery, black-and-white aerial photography, topographic maps, and elevation data. Unit descriptions and stratigraphy were categorized based on prior characterization by Stewart (1999) (Fig. 5). Geochemical analyses of the volcanostratigraphy were presented in Say and Zuza (2020) and are in Figure S1 and Table S1[1].

Say and Zuza (2020) previously presented two $^{40}Ar/^{39}Ar$ hornblende ages from the Pine Nut Mountains, and here we provide new data for nine additional samples to provide a more comprehensive picture of the volcanostratigraphy and bracket cross-cutting deformation. Vikre and McKee (1994) provided other K-Ar whole-rock ages on andesites within the Como Mining District, including 7–6 Ma for andesite flows and 4–3 Ma for the overlying dacitic volcanic rocks.

We collected representative samples from stratigraphy across the study area, choosing homogenous samples with little to no hydrothermal alteration to reduce contamination in argon measurements. Sampling focused on the conformable stratigraphic section in the main portion of the range. Typically, hornblende was preferred for $^{40}Ar/^{39}Ar$ analyses, but when hornblende was not present in the volcanic flows or was highly altered, biotite and/or groundmass was analyzed. Thin sections were observed to evaluate alteration. Argon analyses were conducted at the New Mexico Geochronology Research Laboratory at the New Mexico Institute of Mining and Technology (Socorro, New Mexico) following procedures of McIntosh et al. (2003) and Henry et al. (2017). Samples were irradiated at the U.S. Geological Survey TRIGA reactor in Denver, Colorado.

A summary of new age data with sample locations is in Table 1, age spectra are in Figure 6, and representative stratigraphy with ages from this study is in Figure 5. Complete age data are in Table S2 (footnote 1). All samples displayed relatively flat K/Ca ratios (Table S2), suggesting minimal complications from different phases degassing or inclusions.

Local Stratigraphy with Age Constraints

The oldest units in the northern Pine Nut Mountains are Jurassic metasedimentary and metavolcanic rocks of the Gardnerville Formation (unit J$\bar{T}$g; Noble, 1962; Stewart, 1997) (Fig. 5). The total thickness is not exposed in the study area, and it is possibly more than several kilometers thick (Noble, 1962). Unconformably overlying the Gardnerville Formation is an Oligocene ash-flow tuff (unit Tbt; 67.7% SiO_2) (Fig. 5). Where observed in the northern Pine Nut Mountains, the tuff is 15 m thick and moderately welded with quartz, plagioclase, sanidine, and euhedral biotite phenocrysts. The tuff is tan to pink in color and exhibits lapilli pumice fragments as well as angular andesite clasts as large as 1 cm in diameter. Although we cannot definitively correlate the tuff with other Oligocene ash-flow tuffs exposed in the area, based on its location and phenocryst assemblage, it is most similar to either of the ca. 27 Ma Lenihan Canyon or Mickey Pass Tuffs (e.g., Stewart, 1999; Henry and John, 2013). The relative abundance of biotite and the SiO_2 content are more similar to those of the 26.94 Ma Lenihan Canyon Tuff (Henry and John, 2013).

The dominant lithology consists of Miocene volcanic rocks (Fig. 5). These are intermediate to felsic (~55%–65% SiO_2), calc-alkaline, and predominately metaluminous (Fig. S1 [footnote 1]). All analyzed samples are consistent with a subduction zone setting (e.g., Pearce, 2008; Pearce and Peate, 1995) based on their trace element data (i.e., Nb depletion and Sr, K, and Ba enrichment) and are broadly similar to other studied volcanic rocks associated with the Ancestral Cascade arc around the greater Reno, Nevada, region (Cousens et al., 2008; du Bray and John, 2011; Timmermans et al., 2020). Therefore, we infer that volcanism in the Pine Nut Mountains was related to the Ancestral Cascade arc and preceded Basin and Range bimodal volcanism in the area (e.g., Say and Zuza, 2020). Below we provide a brief overview of the main map units, from oldest to youngest.

Dark gray to gray hornblende dacite (unit Thd; 64%–66% SiO_2) overlies Oligocene tuff and Mesozoic basement rocks (Fig. 5). The dacite is ~250–300 m thick in areas but may be thicker given the concealed contact with adjacent units. Dacite flows contain hornblende, plagioclase, and sparse quartz. Massive, silt-supported black lahar and conglomerate deposits (unit Tcb), as much as 10 m thick, are locally deposited over the dacite in discontinuous incised channels. Limited exposures of porphyritic biotite dacite flows (unit Tbd; 64% SiO_2) occur near the lower portion of unit Thd in the central part of the map area. A similar package of units Thd-Tbd is observed in small exposures in the northwestern corner of the map, in fault contact with stratigraphically higher dacite and andesite flows. Our unit Tbd sample MS-240819-6b collected from this exposure (Fig. 5) yielded a biotite plateau age of 14.20 ± 0.012 Ma (Fig. 6), which is the oldest age obtained in this study, consistent with our interpretation of its low stratigraphic position (Fig. 5).

A 20–30-m-thick gray shale (unit Tss) caps unit Thd (Fig. 7C). The Tss unit thickens to the north with more interbedded diatomaceous shale and sandstone. A volcaniclastic debris flow (unit Tvc1) was deposited over the shale, with subangular to subrounded boulder to cobble sized andesite clasts in a sandy-ash matrix. Above this, the Como andesite (unit Tac; 58%–64% SiO_2) contains andesite flows, interbedded reworked tuff, and pyroclastic flow deposits (unit Tact) (Fig. 5). The Como andesite unit

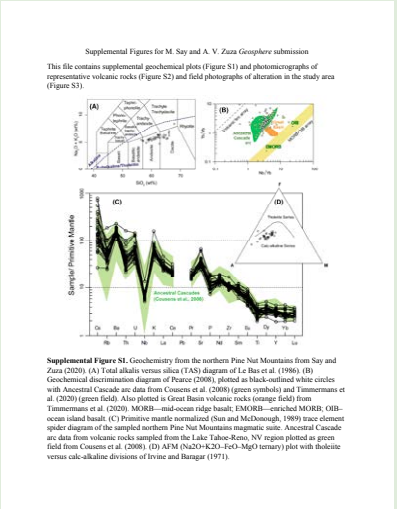
Supplemental Figures for M. Say and A. V. Zuza *Geosphere* submission

This file contains supplemental geochemical plots (Figure S1) and photomicrographs of representative volcanic rocks (Figure S2) and field photographs of alteration in the study area (Figure S3).

Supplemental Figure S1. Geochemistry from the northern Pine Nut Mountains from Say and Zuza (2020). (A) Total alkalis versus silica (TAS) diagram of Le Bas et al. (1986). (B) Geochemical discrimination diagram of Pearce (2008), plotted as black-outlined white circles with Ancestral Cascade arc data from Cousens et al. (2008) (green symbols) and Timmermans et al. (2020) (green field). Also plotted is Great Basin volcanic rocks (orange field) from Timmermans et al. (2020). MORB—mid-ocean ridge basalt; EMORB—enriched MORB; OIB—ocean island basalt. (C) Primitive mantle normalized (Sun and McDonough, 1989) trace element spider diagram of the sampled northern Pine Nut Mountains magmatic suite. Ancestral Cascade arc data from volcanic rocks sampled from the Lake Tahoe-Reno, NV region plotted as green field from Cousens et al. (2008). (D) AFM (Na_2O+K_2O–FeO–MgO ternary) plot with tholeiite versus calc-alkaline divisions of Irvine and Baragar (1971).

[1]Supplemental Materials. Figures S1–S3: Geochemical plots, photomicrographs of representative volcanic rocks dated in this study, and field photographs of alteration in the study region. Table S1: Geochemical analyses. Table S2: Argon dating analyses. Please visit https://doi.org/10.1130/GEOS.S.14981157 to access the supplemental material, and contact editing@geosociety.org with any questions.

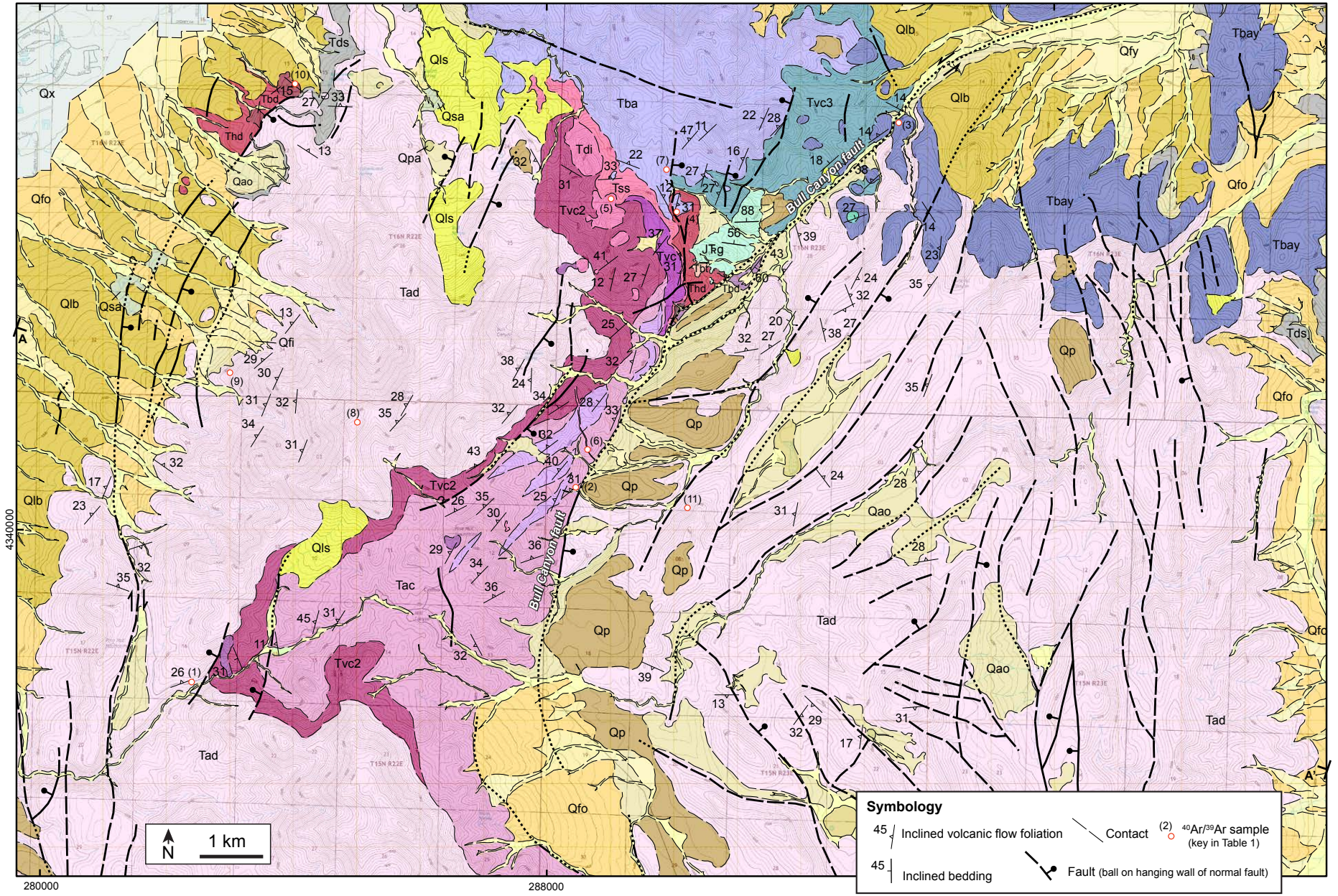

Figure 4. Simplified geologic map of the Pine Nut Mountains, Nevada (adapted from Say and Zuza, 2020). Universal Transverse Mercator zone 11N projection and coordinates. Map location is shown in Figure 1A. Cross-section line A-A′ is for the cross section in Figure 8A. Geologic map units are described in Figure 5.

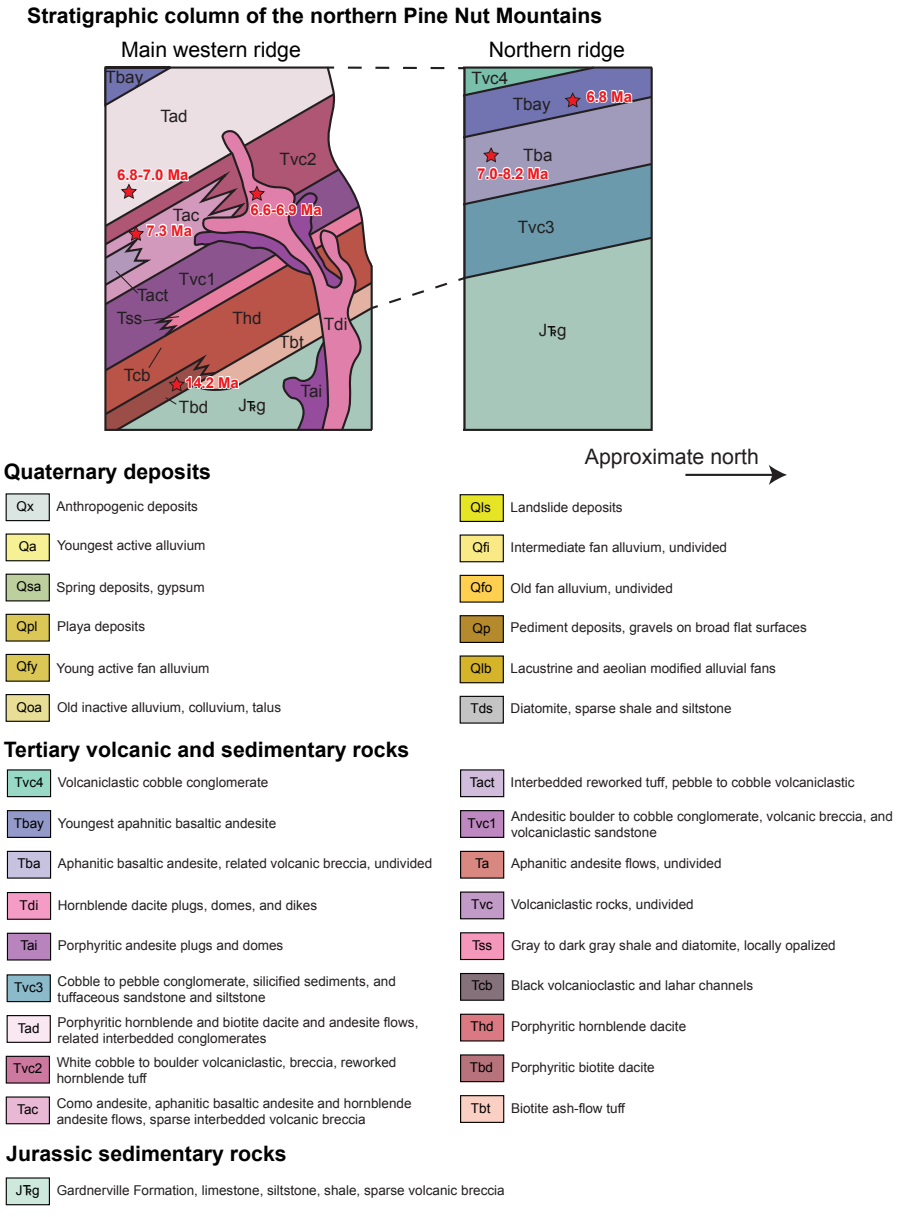

Figure 5. Schematic stratigraphic columns of the northern Pine Nut Mountains showing relative stratigraphic and cross-cutting relationships based on our field observations and Say and Zuza (2020). Red stars indicate units that were analyzed for $^{40}Ar/^{39}Ar$ ages (nine argon ages from this study and two from Say and Zuza, 2020). Geologic unit explanation is for this figure and Figure 4.

is at least 1 km thick but may thin to the north and south. Its lower portions are dominated by andesite lavas, containing plagioclase, pyroxene, and hornblende (Figs. S2A and S2B [footnote 1]), whereas the upper parts are mostly porphyritic andesite to basaltic andesite with sporadic aphanitic flows. Say and Zuza (2020) reported a hornblende $^{40}Ar/^{39}Ar$ age of 7.30 ± 0.09 Ma (sample MS-270918-1; Fig. 6) from the lower Tac unit. In the upper Tac unit, the interbedded, reworked tuff is highly altered and mineralized displaying montmorillonite, quartz, chlorite, and pyrite throughout the unit (Vikre and McKee, 1994).

Overlying unit Tac is white to light brown massive conglomerate, with hornblende-bearing pyroclastic flows, and debris-flow deposits that vary in thickness along strike (unit Tvc2; Fig. 7B). Above this is a mixed unit consisting of dacite, minor interbedded andesite, and debris-flow deposits (unit Tad) (Fig. 5), which is the most widespread unit in the northern Pine Nut Mountains by volume and surface area. In Tad, porphyritic dacite flows are composed of plagioclase, hornblende, biotite, and quartz. Rounded to subrounded xenoliths of dacite to andesite, as large as 20 cm in diameter, are present in outcrops throughout the Tad unit. The upper contact is not exposed in the study area, but the thickness of unit Tad may be >1.5 km.

Four argon dates constrain the age of the Tad unit. Sample MS-070819-4 yielded a $^{40}Ar/^{39}Ar$ biotite age 6.83 ± 0.01 Ma (Fig. 6). Samples MS-230619-1 and MS-030819-1B display highly disturbed spectra (Fig. 6) that may result from hydrothermal alteration of the hornblende phenocrysts. The integrated ages are ca. 10–11 Ma, and the flattest earlier release part of the spectra shows ages of ca. 7–8 Ma. The spectra are generally consistent with other results, but we do not further interpret the disturbed spectra, which may have experienced ^{40}Ar loss due to alteration (Harrison, 1982). Sample MS-261018-2, also from the lower Tad unit, was dated in Say and Zuza (2020) and yielded a hornblende age of 7.15 ± 0.10 Ma. Taken together, dating of the Tad unit suggests an age range of ca. 7.15–6.8 Ma (Fig. 6).

Shallow intrusive rocks (units Tdi and Tai; Fig. 5) and dikes intruded the volcaniclastic debris-flow deposits (unit Tvc2), dacite-andesite flows (unit

TABLE 1. $^{40}Ar/^{39}Ar$ AGES FOR SAMPLES FROM THE NORTHERN PINE NUT MOUNTAINS, NEVADA

Sample	Map label†	Latitude (°N)	Longitude (°W)	Rock unit	Analyzed phase	Preferred age (Ma)	Uncertainty (Ma)
MS-261018-2*	1	39.16056059	119.5180217	Tad	H	7.15	0.10
MS-270918-1*	2	39.18903550	119.4503249	Tac	H	7.30	0.09
MS-220918-1	3	39.24242379	119.3930329	Tbay	G	6.77	0.02
MS-070719-4	4	39.22923559	119.4322926	Tba	G	6.99	0.10
MS-240819-4	5	39.23125276	119.4441570	Tdi	H	6.89	0.05
MS-060419-4	6	39.19499120	119.4474652	Tdi	H	6.59	0.06
MS-240819-3	7	39.23464482	119.4335846	Tba	H	8.20	0.05
MS-230619-1	8	39.19783161	119.4893087	Tad	H	—	—
MS-030819-1B	9	39.20418107	119.5137950	Tad	H	—	—
MS-240819-6b	10	39.24570472	119.5024019	Tbd	B	14.2	0.02
MS-070819-4	11	39.18691433	119.4293465	Tad	B	6.83	0.01

Note: Rock units are described in Figure 5. Analyzed phases: H—hornblende; G—groundmass; B—biotite. Dash indicates sample displayed disturbed spectra and thus no single age is reported. See Figure 6 and Table S2 (text footnote 1) for details.

*Age originally reported in Say and Zuza (2020).

†Refers to sample labels in the Figure 4 geologic map.

Tad), and andesite lavas and tuffs (unit Tac) in the eastern main range (Fig. 7D). A dacite dike (65% SiO_2) intrudes the Como andesite (unit Tac) and reworked tuff unit (unit Tact) and is cut by the major east-bounding normal fault on the eastern flank of the range (Figs. 4 and 7D). New argon analyses from unit Tdi yielded ages of 6.89 ± 0.05 Ma (sample MS-240819-4) and 6.59 ± 0.06 Ma (sample MS-060419-4) (Fig. 6). These ages overlap ages from the Tad unit, described above, and thus may reveal a connection between units Tdi and Tad. Unit Tdi intruded the stratigraphically lower portions of unit Tad, but based on age relationships and spatial position, we interpret that unit Tdi may have been genetically related to the erupted andesite and dacite flows in the middle and upper Tad unit (Fig. 5).

In the northernmost Pine Nut Mountains, there are poorly exposed and silicified volcaniclastic debris flows, cobble conglomerates, tuff beds, and tuffaceous sedimentary rocks (unit Tvc3; Fig. 5) that overlie the Jurassic Gardnerville Formation (Fig. 4). Aphanitic basaltic andesite flows (unit Tba; 56%–59% SiO_2), composed of a glassy groundmass, plagioclase, and clinopyroxene, overlie Tvc3. Two $^{40}Ar/^{39}Ar$ analyses from unit Tba display plateau ages of 6.99 ± 0.10 Ma (sample MS-070719-4) and 8.20 ± 0.05 Ma (sample MS-240819-3) (Fig. 6). The two sample locations are separated by a poorly exposed interpreted fault, and therefore comparison of their ages is not straightforward (Fig. 4). The older age for sample MS-240819-3 (hornblende age: 8.20 ± 0.05 Ma) is consistent with its position in the footwall of a normal fault, compared to the younger age for sample MS-070719-4 (groundmass age: 6.99 ± 0.10 Ma). We caution that discrepancies between the analyzed phases—hornblende for the older age versus variable-composition groundmass, mostly plagioclase, for the younger age—preclude using the age difference for a meaningful estimate of fault displacement. The closure temperature for Ar diffusion in the finer-grained plagioclase groundmass (sample MS-070719-4) (i.e., 225–300 °C nominal closure temperature for plagioclase) (e.g., Harrison, 1982; McDougall and Harrison, 1999; Cassata et al., 2009) was probably lower than for hornblende, which made sample MS-070719-4 more susceptible to later heating.

The youngest aphanitic basaltic andesite (unit Tbay) was deposited with a slight angular unconformity over the dacite-andesite flows and unit Tvc3 (Fig. 4). The aphanitic basaltic andesite flows have plagioclase, clinopyroxene, orthopyroxene, and a glassy groundmass (Figs. S2E and S2F [footnote 1]). An analysis on groundmass material (sample MS-220918-1) yielded an age of 6.77 ± 0.02 Ma (Fig. 6)—younger than the units that the Tbay unit was deposited on (units Tba and Tad in the northeastern portion of the map area; Fig. 4)—which supports the stratigraphic interpretation of unit Tbay being younger than the other flow units (Fig. 5).

Structural Observations in the Northern Pine Nut Mountains

Faults in the Pine Nut Mountains study area generally strike north and dip east (Fig. 4). The major north-striking fault on the eastern flank of the main range, here referred to as the Bull Canyon fault, dips east and has a fairly continuous, curvilinear fault trace (Fig. 4). This fault strikes north along its southern strand and gradually bends to a northeast strike along its northern strand. The Bull Canyon fault cuts the entire stratigraphic section exposed in the northern Pine Nut Mountains. A ca. 6.6 Ma (sample MS-060419-4; this study) dacite dike (unit Tdi) (Fig. 7D) is truncated by the Bull Canyon fault on the eastern flank of the main range (Fig. 4). Fault striations observed along the southern strand (Fig. 7F) suggest mostly dip-slip kinematics (average striation trend/plunge: 070°/40°), whereas the northern strand has subhorizontal striations suggesting some oblique lateral component of slip (average striation trend/plunge: 030°/10°) (Fig. 4).

The prominent range in the western part of the map area has tilted volcanic flows and interbedded sedimentary rocks that dip an average of 30° northwest (Fig. 4). The westward tilting of the stratigraphy is interpreted here to have resulted from vertical displacement along the range-bounding, east-dipping Bull Canyon fault (Fig. 4). The youngest dated volcanic unit from the conformable volcanostratigraphy yielded a $^{40}Ar/^{39}Ar$ age of 6.83 ± 0.01 Ma (sample MS-070819-4). We interpret that dip-slip normal faulting and extension initiated in the Pine Nut Mountains after ca. 6.8 Ma, after the eruption and deposition of the conformable dacite and andesite flows (unit Tad) (Fig. 6). This suggests that the 30°–36° of northwest tilting of the main range occurred at a bulk tilting rate of 4.4°–5.3° $m.y.^{-1}$.

North-striking curvilinear faults cut Quaternary fans on the western flank of the Pine Nut

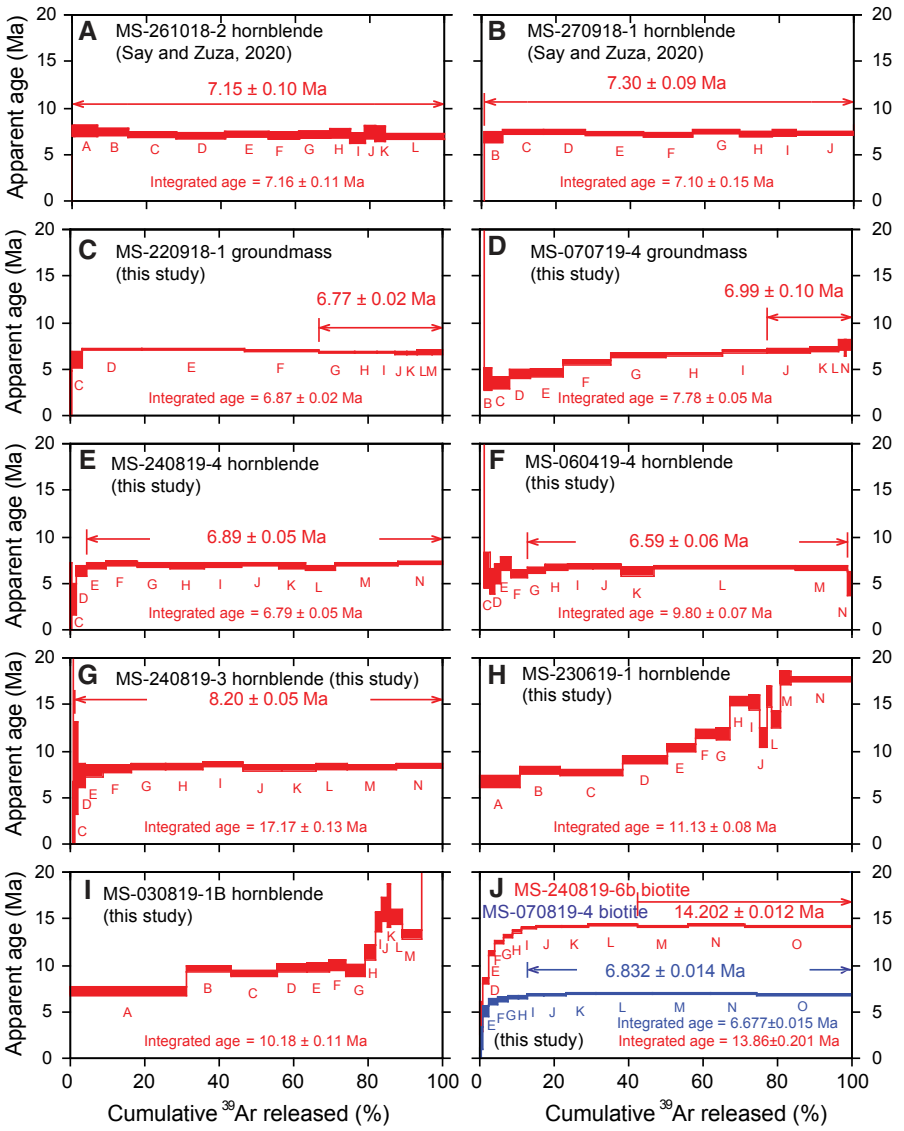

Figure 6. $^{40}Ar/^{39}Ar$ step plots displaying plateau (plateau marked with arrows) and integrated ages of eleven samples. See Table 1 for age summary and Supplemental Table S2 (text footnote 1) for complete data. Data plotted at 2σ and results at 1σ.

Mountains (Say and Zuza, 2020). We previously interpreted that these uphill-facing (east-dipping) scarps (Fig. 4) may have a significant right-lateral slip component that cuts lacustrine-modified alluvial fans and shoreline deposits (unit Qlb) but is covered by units Qfy, Qfi, and Qfo. Based on surficial characteristics and shoreline elevations higher than, and thus older than, those of the ancestral Late Pleistocene Lake Lahontan (~1338 m; Adams and Wesnousky, 1998), we suggest that these faults are Middle to Late Pleistocene in age. These minor active faults may be part of the distributed right-slip fault network accommodating small fractions of the 10 mm yr^{-1} right-lateral shear that is observed geodetically (Kreemer et al., 2009; Bormann et al., 2016), as envisioned by Pierce et al. (2021).

Hydrothermal Alteration

Hydrothermal alteration of various types and degrees is prevalent in the northern Pine Nut Mountains. The historic Como Mining District is in the study area, centralized around the Como townsite. Recently, expanded explorations (new drilling as of 2020) have been started around the Como townsite and to the north in the Hercules property. The Como andesite (unit Tac) is the host rock for the majority of the observed alteration. Areas north of the Como Mining District also exhibit alteration in the overlying dacite unit (unit Tad) and volcaniclastic sediment deposits (unit Tvc3). Alteration mineral assemblages were not categorized in this study but have been described in previous work by Vikre and McKee (1994) and Russell (1981).

Propylitic alteration in the Como area is the most pervasive alteration type in the study area. Propylitic alteration is the most noticeable due to the dull green, blue, and purple colors displayed throughout the Como andesite (unit Tac; Figs. S3A and S3B [footnote 1]) and is confined to the more permeable interbedded volcaniclastic, volcanic breccia, and lahar-type deposits within the andesite unit (unit Tact). Propylitic alteration destroyed much of the original texture and bedding in these units, which resulted in irregular platy fracturing

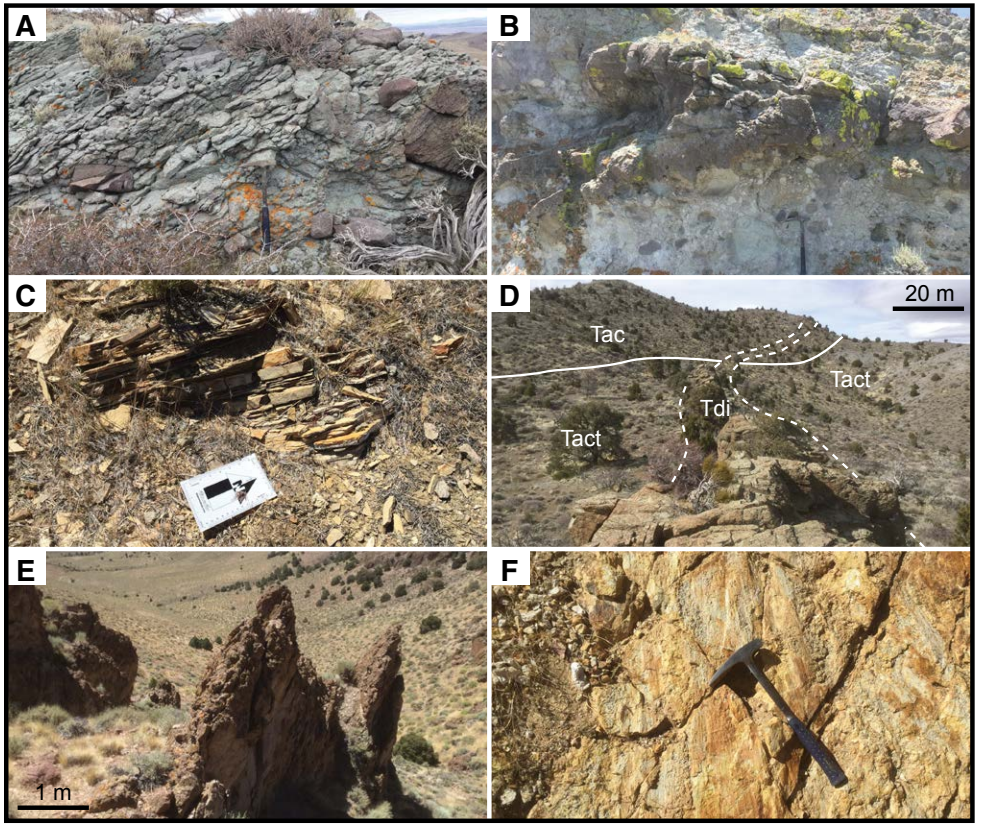

Figure 7. Field photographs showing important relationships and observations. (A) Subangular to subrounded andesite cobbles in matrix of foliated reworked tuff unit Tact (40 cm rock hammer for scale). (B) Cross bedding in conglomerate, pyroclastic, and debris-flow unit Tvc2 (40 cm rock hammer for scale). (C) Typical exposure of thinly bedded shale unit (Tss) (white card is 10 cm long). (D) Hornblende dacite dike (unit Tdi) that is truncated on the eastern side by the Bull Canyon fault and intrudes the Como andesite (unit Tac) and reworked tuff (unit Tact) units (view looking west). $^{40}Ar/^{39}Ar$ age on the dacitic dike yielded 6.59 ± 0.06 Ma. (E) Brecciated, erosion-resistant northeast-striking fault plane in the northern range (view looking southwest). (F) Dip-slip striations along the north-striking section of the Bull Canyon fault (40 cm rock hammer for scale; view looking northwest). Please add the following to convey the location information: Photograph locations: (A) 39°11′30.79″N/119°27′6.11″W; (B) 39°12′57.05″N/119°26′14.65″W; (C) 39°13′1.59″N/119°25′49.82″W; (D) 39°11′47.04″N/119°26′52.22″W; (E) 39°14′28.23″N/119°24′48.12″W; (F) 39°11′7.80″N/119°27′0.83″W.

that makes it difficult to distinguish between relict bedding and alteration-created fracturing (Fig. 7A).

Argillic and acid-sulfate alteration is pervasive in the southeastern portion of the Como Mining District and adjacent to silicified fault zones. Argillic and acid-sulfate alteration are confined to the Como andesite. Argillic alteration is not well exposed due to the erodible nature of the altered outcrops (Fig. S3C [footnote 1]). In locations where they are exposed, highly bleached andesite and interbedded volcaniclastic deposits display voids of leached plagioclase. Kaolinite is present along with other unidentified clays in areas of argillic alteration (Vikre and McKee, 1994). Acid-sulfate alteration is present in andesite flows and the interbedded volcaniclastic deposits, similar to the argillic alteration. Exposures of the acid-sulfate alteration occur as highly bleached and erosion-resistant knobs of andesite (Fig. S3D).

The ore-bearing alteration assemblage and historic production in the Como Mining District are located in silicified faults and veins (Russell, 1981). Silicified fault and veins vary in orientation but mostly strike north-northeast. The silicified faults are well exposed in the district and occur as resistant ribs of relatively high relief and are as much as 10 m wide (Figs. S3E and S3F [footnote 1]). Quartz is the dominant gangue mineral with sparse calcite, and some fault zones large cavities of prismatic quartz crystals as large as 1 cm. Float of prismatic, botryoidal, colloform, and acicular quartz is found around the Como andesite unit and is possibly from concealed veins. Almost all of the mineralized fault zones display striations indicating some post-mineralization faulting.

Veins in the Como Mining District are more discrete than the silicified faults. Outcrops of veins are exposed, primarily from past prospecting, as rubbly float of quartz and calcite. K-Ar dating on K-feldspar and alunite yielded a mineralization age of 6–7 Ma (Vikre and McKee, 1994). This age agrees with the age of the Como andesite of 7.3 Ma (sample MS-270918-1; Say and Zuza, 2020), which indicates that alteration quickly followed deposition of the volcanic flows and may be associated with heat supplied from volcanic vents in the area. The mineral assemblage of the veins and silicification in the Como Mining District would suggest a high-sulfidation-type epithermal deposit (Ridley, 2013). However, numerous silicified faults and veins and large amounts of silicified quartz breccia in the northeastern portion of the study area may represent a more low-sulfidation-type epithermal deposit influenced by meteoric water. On a larger scale, mineralization and alteration are confined to the footwall of the Bull Canyon fault within the Pine Nut Mountains on the eastern flank of the range and stratigraphically below younger dacite and andesite flows (unit Tad; Fig. 4). Therefore, mineralization

may have occurred prior to the eruption and deposition of unit Tad, or it was simply confined to stratigraphically deeper layers. It appears that mineralization occurred prior to the displacement along the main eastern range-front fault (Fig. 4).

TIMING, MAGNITUDE, AND RATE OF EXTENSION IN THE PINE NUT MOUNTAINS

Magnitudes of extension were estimated from our construction of a new cross section across the northern Pine Nut Mountains (Fig. 8A), which we compare with a cross section constructed by Long (2019) across the central Pine Nut Mountains (Fig. 8B). Our cross section was constructed along a northwest-trending profile through the study area using surficial structural data and stratigraphic relationships recorded from geologic mapping (Fig. 4). The cross section adheres to map relationships and stratigraphic observations, and was restored to a pre-deformed state to allow quantification of the minimum magnitude of late Cenozoic extension that affected the range (Fig. 8). The line-balancing method was used to restore the deformation in the restored section. It was assumed that stratigraphic thickness in the subsurface is constant, which may not always be true due to variations in thickness along strike for certain lithologies in the map area (Fig. 4). We adhered to field and map relationships as best as possible when projecting contacts to depth. Based on stratigraphic observations, some units in the cross section are discontinuous or are intertongued with other units (e.g., units Tact, Tss, Tbd, and Tbt). Nonetheless, the units that contain these discontinuous or intertongued units (e.g., units Tac, Tvc1, and Thd) appear to remain a constant integrated unit thickness at the scale of our cross-section models. Another uncertainty is the geometry of the stratigraphy in the subsurface along the easternmost portion of the section line (Fig. 8A). Only limited structural data from this region of the map area provide the amount of tilt of the stratigraphy (Fig. 4). Based on sparse structural measurements and satellite imagery, we assumed a 15°W dip for the Tad unit and underlying stratigraphy to achieve the constant exposure of the Tad unit at the surface (Fig. 4) in the eastern portion of the section line (Fig. 8A). Large offsets along east-dipping faults and negligible offsets on west-dipping faults in the eastern portion of the section were also assumed to match mapped bedrock exposure at the surface, such as for unit Tad (Fig. 8A). Poor exposures of units Tbd and Thd in the foothills west of the range suggest another relatively large-displacement normal fault, but these field relationships are unclear due to poor exposure and overlying basin sediments (Fig. 4). The possibility of oblique slip on this fault makes fault-slip reconstructions here ambiguous.

Our preferred line-length restoration was based on the cross section drafted to the western limit of the main range, which yielded a minimum magnitude of late Cenozoic extension of 2.5 km (14% minimum extensional strain; Fig. 8A). Using the poorly exposed Tbd and Thd units west of the range permits a longer cross section that would yield a line-length extension magnitude of ~3.7 km (20%). We prefer the 2.5 km extension estimate to keep our constraints at minimum extension magnitudes. The largest sources of uncertainty in this estimate are original fault dips, which are constrained based on cutoff relationships and our inferences on the subsurface geology, which are in turn best constrained by lateral map relationships. To test these extension estimates and evaluate potential uncertainties based on the choice of original fault dips, we calculated the expected extension magnitude for rigid-block rotation of the main range using a derivation from McKenzie and Jackson (1983). Assuming 30° westward tilting of the main range, a block width of ~6 km, and initial fault dips ranging from 65° to 75°, we calculate extension magnitudes of 2–2.5 km. This value is similar to our line-length-restoration extensional strain estimate.

Figure 8B shows the cross section from Long (2019) across the central Pine Nut Mountains, south of our mapped area (Fig. 1B). This section was constructed based on geologic constraints from Stewart (1999) and Cashman et al. (2009). We minimally modified this section to the scale of our section in Figure 8A, and our line-length extension estimates of the Cenozoic unconformity surface suggest 2.8 km extension (13% minimum extensional strain; Fig. 8B). Long (2019) previously reported 4.1 km of extension (20%) from this section based on slightly different picks for the pre-deformed length of the section. The two cross sections discussed above show remarkably similar extension magnitudes, which adds confidence to the strain estimates.

Using our interpretation that extension initiated after ca. 6.8 Ma, our extension estimate equates to an extensional rate of ~0.4 mm yr^{-1}. This rate is a minimum extension rate because our extension estimates are minimum values, deformation may have initiated more recently than ca. 6.8 Ma, and extension may have ceased before the present. The corresponding extensional strain rate is 6.5×10^{-16} s^{-1} across the 17.5 km restored section (Fig. 8A). Using an alternative, greater extension estimate of 3.7 km (20% strain) (Fig. 8A) yielded extension and extensional strain rates of 0.5 mm yr^{-1} and 9×10^{-16} s^{-1}, respectively. These strain rates are comparable to published geodetic strain rates of 9×10^{-16} s^{-1} to 3×10^{-15} s^{-1} in the Walker Lane (Kreemer et al., 2009, 2012). Dilles and Gans (1995) derived faster extensional strain rates of ~10^{-14} s^{-1} for the earlier rapid phase of extension around Yerington.

For comparison and validation, we note that the AFT analyses of Surpless et al. (2002) from south of our study area reveal that their four samples were in the AFT partial annealing zone (60–100 °C; Gleadow et al., 2002; Ketcham et al., 2007) at ca. 41–53 Ma, which equates to depths of 2–4 km assuming thermal gradients of 25–30 °C km^{-1}. Assuming minimum exhumation started ca. 6.8 Ma (i.e., samples started at the cooler end of the partial annealing zone) along an ~60°-dipping normal fault, this equates to an extension rate of 0.5–0.6 mm yr^{-1}. Together, our new observations and published data favor extension rate estimates of 0.4–0.6 mm yr^{-1} across the Pine Nut Mountains since ca. 6.8 Ma. Deformation could have initiated more recently than deposition of the youngest conformable ca. 6.8 Ma volcanic rock, which would increase these rates. For example, if Stockli (1999)'s estimate of ca. 4 Ma exhumation of the Carson Range to the west of the Pine Nut Mountains bears on deformation

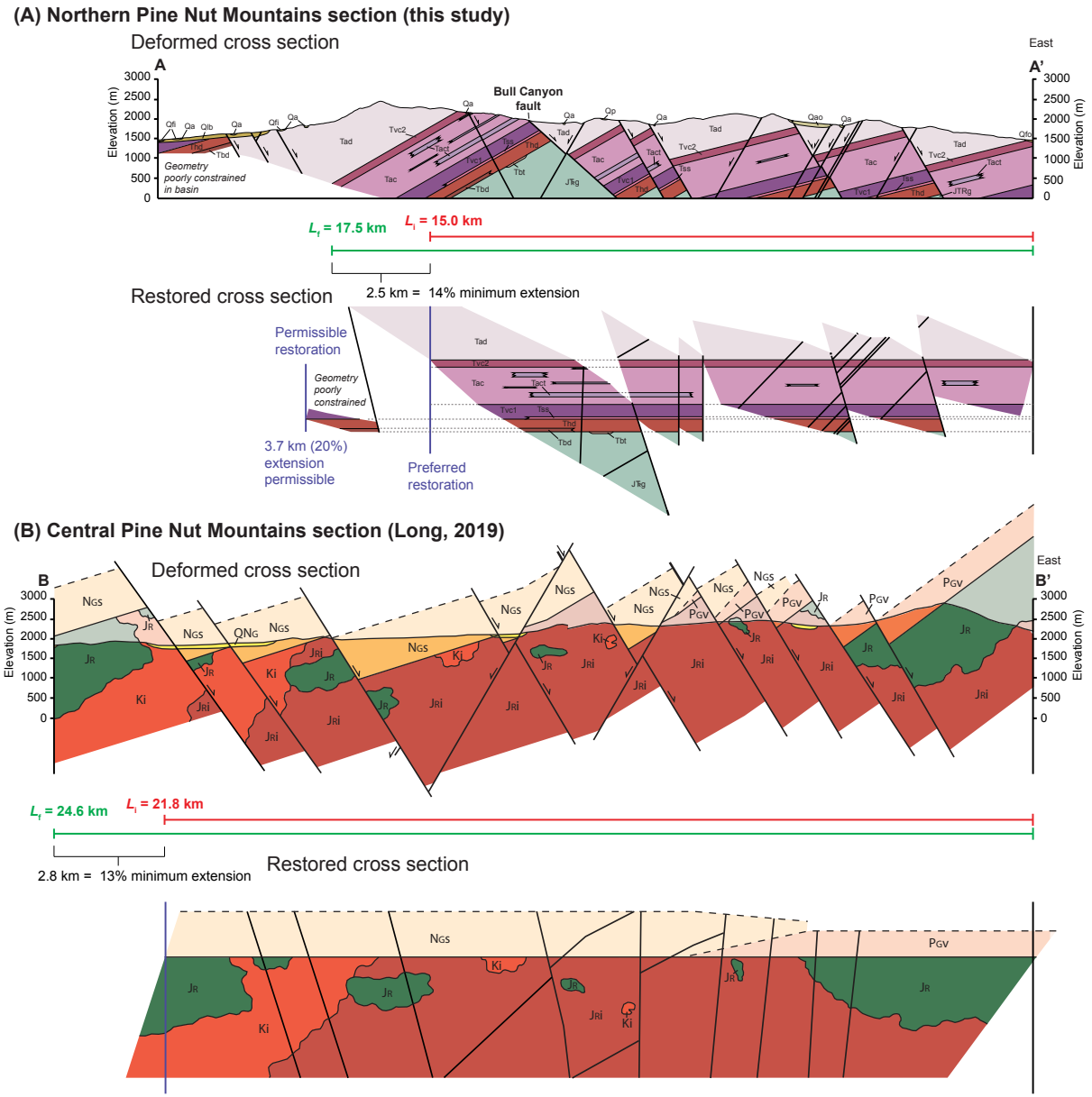

Figure 8. Deformed-state (final length, L_f) and restored cross sections (initial length, L_i) across the northern (A) and central (B) Pine Nut Mountains. Cross section in A is from this study (section line in Figs. 1 and 4), and cross section in B is modified slightly from Long (2019) (section line in Fig. 1). Geologic units shown in A are described in Fig. 5 and see Long (2019) for geologic units in B.

in the Pine Nut Mountains, a faster extension rate of ~0.6 mm yr^{-1} is estimated.

DISCUSSION

Miocene Westward Migration of Basin and Range Extension

Extension in the Pine Nut Mountains is accommodated via high-angle normal faulting, spaced fairly regularly at ~1 km, and block rotation as observed in the cross sections from this study and Long (2019) (Fig. 8). Normal faults initiated at dip angles of 60°–70°, and the most significant faults dip east. Most dip-slip displacement is ≤1 km, with rare faults having displacement of as much as ~2 km. This style of extension is similar to the classic normal-fault system in the Singatse and Wassuk Ranges to the east, which also consists of regularly spaced (1–2 km), high-angle normal faults that initiated at 60°–70° dips (e.g., Proffett, 1977). However, in the Singatse and Wassuk Ranges, the normal faults involved as much as 4 km offset and were rotated to shallow dips, thus accommodating much higher extension magnitudes, >150% (Fig. 9).

Based on our new age constraints, we interpret a broad pattern of westward encroachment of Basin and Range extension against the Sierra Nevada since ca. 14 Ma; deformation first concentrated in the Singatse and Wassuk Ranges and migrated westward to the Pine Nut Mountains after ca. 6.8 Ma, based on our observed conformable package of pre–6.8 Ma volcanic rocks (Dilles and Gans, 1995; Henry and Perkins, 2001; Surpless et al., 2002) (Fig. 9). The Singatse and Wassuk Ranges experienced rapid extension (~10^{-14} s^{-1}) from ca. 14 to 12.5 Ma (Dilles and Gans, 1995; Surpless et al., 2002). Normal faulting in the Pine Nut Mountains after ca. 6.8 Ma is consistent with AFT data from Surpless et al. (2002) (Fig. 9B). Just west of the Pine Nut Mountains, sediments in the Neogene Gardnerville Basin were deposited from ca. 7 to 2 Ma (Muntean, 2001; Cashman et al., 2009). In the Gardnerville Basin, deposits dip west and paleoflow measurements show mostly west-directed deposition, thus indicating that they were derived from the uplift of the Pine Nut Mountains (Cashman et al., 2009). To the west in the Carson Range, extension initiated sometime after ca. 10 Ma (Henry and Perkins, 2001; Surpless et al., 2002; Cashman et al., 2009) (Fig. 9). The best local constraint is from Stockli (1999)'s AHe traverse, which suggests ca. 4 Ma exhumation of the Carson Range.

There are some complications to the kinematic model presented in this study. Dilles and Gans (1995) discussed a phase of ca. 23 Ma ancestral Walker Lane transtensional deformation around Yerington. All strata and deformation recorded in our study area are younger than this late Oligocene phase of deformation; thus, there is no record of late Oligocene deformation. Accordingly, we refrain from making interpretations about an earlier phase of deformation. In addition, Henry and Perkins (2001) documented earlier sedimentation in the Verdi-Boca Basin ca. 12 Ma that may reflect dip-slip normal faulting initiation and basin generation. The Verdi-Boca Basin was later deformed with renewed ca. 3 Ma extension. We found no evidence of 12 Ma basin sedimentation or constraints for coeval deformation. Our oldest Cenozoic map unit yielded an age of 14.2 Ma, and therefore there may be ca. 12 Ma volcanic strata that were not dated (Fig. 6).

Transtension Initiation

Walker Lane right-lateral transtensional deformation followed Basin and Range dip-slip extension in the Pine Nut Mountains sometime after ca. 6.8 Ma. Prior studies suggested that Walker Lane transtension in the Carson domain initiated between 9 and 5 Ma (Cashman and Fontaine, 2000; Faulds et al., 2005; Faulds and Henry, 2008; Sturmer and Faulds, 2018), which is compatible with our interpretation of extension initiation after ca. 6.8 Ma and Walker Lane transtension starting sometime afterward. Integrating our observations with those of previous studies suggests a constraint on the initiation of Walker Lane deformation between 5 and 6.8 Ma.

Previously unknown Walker Lane structures are preserved in the northern Pine Nut Mountains. We interpret that the northeast-striking strand of the Bull Canyon fault may have accommodated Walker Lane transtension and/or rotational deformation. We posit that left-slip motion may have been kinematically linked with east-dipping dip-slip normal fault motion along the north-striking strand of the fault (Say and Zuza, 2020). This Bull Canyon fault system may have initiated as a dip-slip normal fault during earlier Basin and Range extension that was later reactivated as an oblique-left-slip fault during Walker Lane transtension. In this scenario, the north-striking curvilinear normal fault was produced during Basin and Range extension after ca. 6.8 Ma. Following the onset of Walker Lane northwest-trending right-lateral shear after ca. 6.8 Ma, clockwise vertical-axis rotation of the Carson domain rotated the northern portions of the fault into a northeast orientation more kinematically favorable for left-slip displacement during clockwise block rotation. Alternatively, the present-day fault orientation originated during the initiation of extension and has since been slightly modified by Walker Lane deformation. Sturmer and Faulds (2018) interpreted a similar kinematic history for the Olinghouse fault to the north (Fig. 1). The inferred left-slip Bull Canyon fault is parallel to the three northeast-striking left-slip faults in the Carson domain (Figs. 1 and 3) (i.e., Olinghouse fault and Carson and Wabuska lineaments; Li et al., 2017; Sturmer and Faulds, 2018; Zuza and Carlson, 2018) and thus may have been part of this parallel strike-slip fault system (Zuza et al., 2017; Yang et al., 2020). However, the main range-bounding and northeast-striking strands of the Bull Canyon fault do not displace unit Qao and younger deposits and are therefore not active faults (Fig. 4).

Extension Kinematics and Relationship to North American Plate Boundary

When integrated with data from other published studies, our data reveal two phases of late Cenozoic extension in the study region, just east of the Sierra Nevada: a phase of large-magnitude, fast extension ca. 15–13 Ma (Dilles and Gans, 1995; Surpless et al., 2002), followed by relative tectonic quiescence

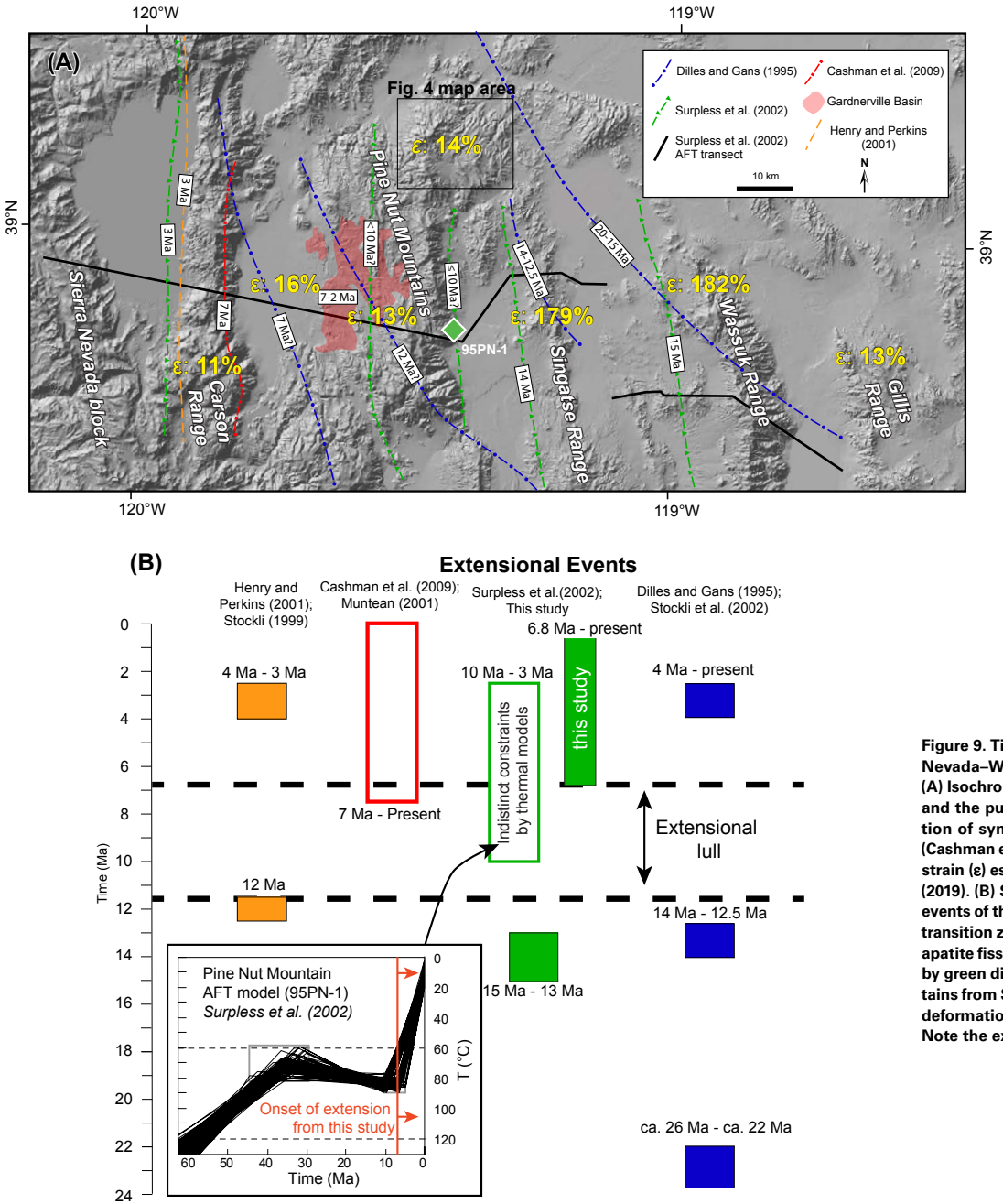

Figure 9. Timing constraints for deformation in the Sierra Nevada–Walker Lane–Basin and Range transition zone. (A) Isochron map of deformational events from this study and the published literature. Red polygon is the distribution of syntectonic 7–2 Ma Gardnerville Basin deposits (Cashman et al., 2009). Yellow text is horizontal extensional strain (ε) estimated in this study, Proffett (1977), and Long (2019). (B) Studies indicating initiation age of extensional events of the Sierra Nevada–Walker Lane–Basin and Range transition zone. Inset shows modeled thermal history from apatite fission track (AFT) sample 95PN-1 (location shown by green diamond in A) from the northern Pine Nut Mountains from Surpless et al. (2002), with orange line showing deformation constraint from this study (*T*—temperature). Note the extensional lull ca. 12–7 Ma.

during the deposition of conformable, subhorizontal, and parallel middle Miocene volcanic rocks, then renewed extension after 6.8 Ma (Fig. 9). The implied punctuated extensional history can help resolve the dominant driver of regional extension. For example, extensional collapse related to elevated gravitational potential energy (GPE) associated with thickened crust (e.g., Sonder and Jones, 1999) or thermal weakening (Surpless et al., 2002) would predict more progressive and continuous extension at the scale of the orogen. Admittedly, this collapse could be variably partitioned across the orogen such that the entire orogen did not extend at once, but observations of lateral motion in the Tibetan Plateau today suggest that such strain should be relatively homogenous (e.g., England and Molnar, 1997; Zuza et al., 2020b). Instead, we suggest that the apparent two-phase kinematic history is best interpreted as a result of changing plate-boundary conditions. When the first-observed phase of rapid extension (~10^{-14} s^{-1}) initiated ca. 15 Ma, the Mendocino triple junction was still significantly south of the study area (DeMets and Merkouriev, 2016), and thus deformation would have been controlled by plate-boundary stresses across the Juan de Fuca–North American plate boundary (e.g., Atwater, 1970; Faulds and Henry, 2008; Lee et al., 2020). Lee et al. (2020) interpreted westward trench retreat at this time, which, when coupled with elevated GPE of the thickened crust, would have allowed for an early phase of fast extension. This initial burst of high-strain-rate extension of thickened crust would have occurred as plate boundary stresses relaxed due to subduction rollback (e.g., Colgan and Henry, 2009; Lee et al., 2020). Alternatively, Nicholson et al. (1994) speculated that consumption and capture of oceanic microplates could lead to discrete jumps of transform-margin elongation, and it is possible that such events could have led to punctuated continental extension (e.g., Stock and Lee, 1994). However, the most time-correlative microplate-capture event was of the Arguello microplate ca. 17.5 Ma (Nicholson et al., 1994), which is earlier than the deformation observed in this study (Fig. 9). Future improvements or refinements to the temporal resolution of these microplate subduction events may reveal a link to pulsed deformation in the western Basin and Range.

After fast extension, an extensional lull occurred due to plate-boundary conditions inhibiting further extension and lower GPE gradients, with renewed slower extension after ca. 6.8 Ma as the Mendocino triple junction migrated northward (DeMets and Merkouriev, 2016). At this time, the plate boundary west of the study region became a transform margin accommodating northwest stretching of Great Basin crust.

Our hypothesis that the ca. 12–7 Ma extensional lull reflects regional plate-boundary events predicts that this tectonic quiescence should have occurred at a regional scale. Slightly longer extensional lulls (ca. 12–4 Ma) are observed in the Wassuk Range (Stockli et al., 2002) and northern Carson Range (Henry and Perkins, 2001) (Fig. 9). There are numerous locations where extension has been inferred to have started ca. 15 Ma (e.g., Henry and Perkins, 2001; Stockli et al., 2002; Colgan et al., 2008, 2020), but we are not aware of definitive constraints on post–7 Ma accelerated or renewed extension that support the existence of our proposed extensional lull on a regional scale. Constraining a younger phase of deformation may be more challenging due to the lack of latest Miocene–early Pliocene (e.g., 7–5 Ma) volcanic rocks across large portions of the western Basin and Range (e.g., Cousens et al., 2008; du Bray and John, 2011). Future focused structural investigations in locations that do contain younger phases of Ancestral Cascades volcanic rocks may better resolve this topic.

Decoupled Upper and Lower Crust and Extensional Strain Transfer

Our refined kinematic history for the Sierra Nevada–Basin and Range transition at the latitude of ~39°N (Fig. 9) permits a high-resolution perspective on upper-crustal extension in the western Great Basin. In particular, magnitudes of Cenozoic extension are highly variable across our studied traverse, from the Carson Range in the west to the Gillis Range in the east, varying significantly from >150% to <15% (e.g., Surpless et al., 2002; Cashman et al., 2009; Long, 2019; this study) (Fig. 9A). This strain heterogeneity is analogous to more regional strain variations across the Great Basin, where deformation is partitioned horizontally and laterally (i.e., in map view) within zones of higher and lower extensional strain (e.g., Coney and Harms, 1984; Long, 2019). This intraplate deformation ultimately accommodates relative plate motion, either via strain discretization on faults that separate rigid-block motion or as local strain concentrations in a deforming continuum (e.g., Molnar and Tapponnier, 1975; England and Houseman, 1986; Avouac and Tapponnier, 1993; Flesch et al., 2000). If upper-crustal strain estimates reflect vertically coherent pure-shear extension, they imply crustal thinning on heterogenous wavelengths that are not compatible with our knowledge of crustal thickness through time. This requires efficient strain partitioning across the vertical crustal column, smoothing strain heterogeneities to match the assumed vertically coherent and uniform horizontal velocity boundary conditions prescribed by relative plate motion.

The initial crustal thickness in the Mesozoic at our study transect was ~60–70 km as constrained by analogy with other arc-plateau systems (Beck et al., 1996; Ryan et al., 2016) and arc mass-balance considerations (e.g., Cao and Paterson, 2016). Geochemical proxies also show that that the Sierra Nevada arc system was 60–70 km thick in the Late Cretaceous (Profeta et al., 2015). Following late Cenozoic extension, the present-day crustal thickness is also well constrained to 30–40 km via seismic reflection profiling (e.g., Allmendinger et al., 1982; Surpless et al., 2002) and modern geophysical surveying (e.g., Gilbert, 2012). Both Mesozoic and present-day crustal thickness estimates suggest relatively smooth Moho horizons, such that there are not significant jumps in crustal thickness values from west to east. Following similar logic to Gans (1987), we can use estimates of Cenozoic extension to evaluate the evolution from Mesozoic to present-day crustal thickness.

For this exercise, we use the framework setup of Long (2019), including their synthesis of extension magnitudes, integrating our observations from the Pine Nut Mountains (Fig. 10). We consider the region from the Carson Range in the west to the Gillis Range in the east (Figs. 1 and 10), which has present-day crustal thickness estimates of 30–40 km

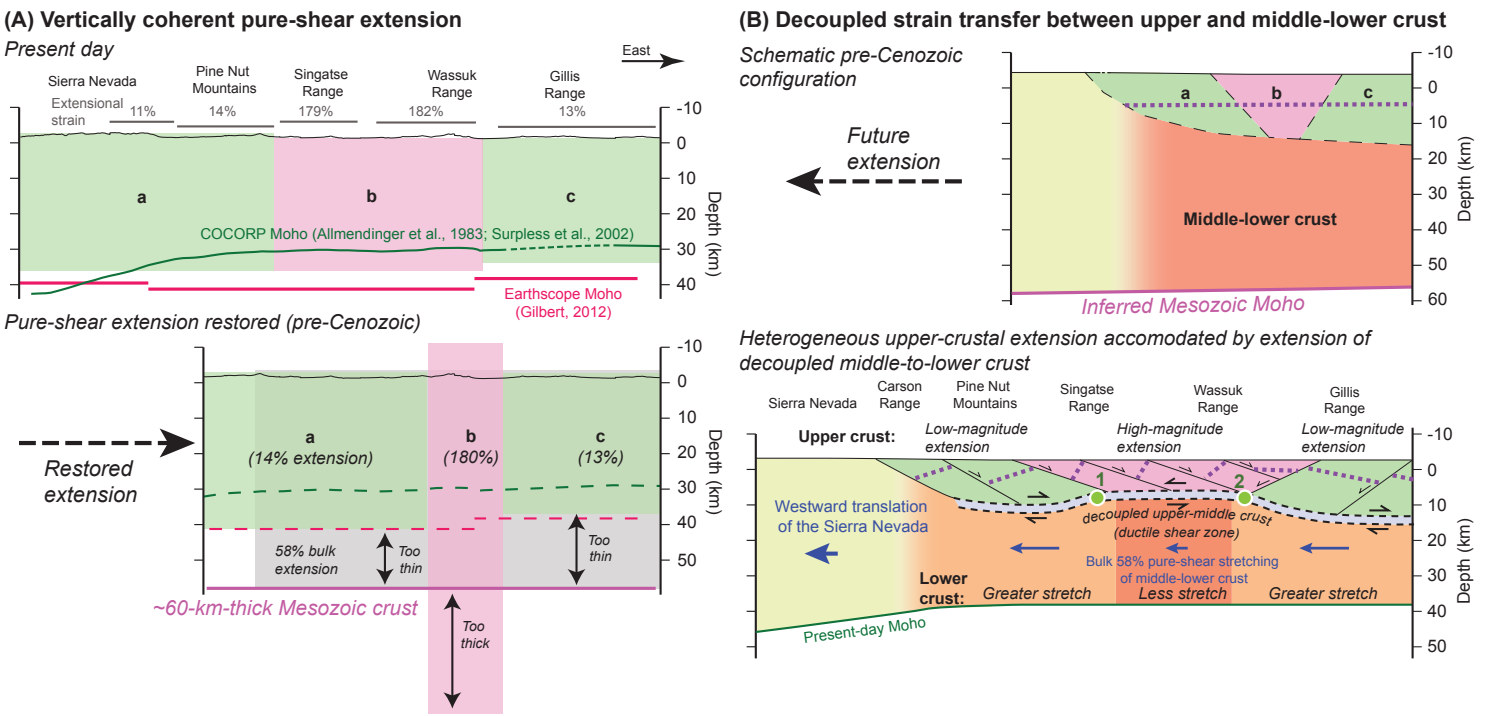

Figure 10. Schematic cross sections across the Sierra Nevada–Basin and Range transition at the approximate latitude of 39°N, demonstrating the relationship between Cenozoic extension and the pre-extensional Mesozoic crustal thickness. (A) A vertically coherent pure-shear model of extension is problematic in relating pre- and post-extension crustal thickness estimates with observations of extensional strain. The present-day crustal thickness is shown in a crustal-scale cross section (modified from Long, 2019) using crustal thickness values from Gilbert (2012) (red) and the COCORP-derived Moho depth (green; Allmendinger et al., 1983; Surpless et al., 2002). Estimates of Cenozoic crustal extension are shown in gray as a percentage, with the bar length symbolizing the approximate region of extension (from Long [2019], except for the Pine Nut Mountains, from this study). Estimates of extension define three domains—i.e., a, b, and c—that alternate low and high extensional strain. Pure-shear restoration of these domains to approximate Mesozoic crustal thickness results in crust that is either too thick or too thin. This study assumes that the Mesozoic crustal thickness in this study area was ~60 km (or greater) based on analogy to the Andes (e.g., Ryan et al., 2016) and mass-balance considerations of the Sierra Nevada arc (Cao and Paterson, 2016). Note that restoration of homogenous pure-shear extension across the region can reasonably recreate the Mesozoic crust thickness assuming 58% bulk extension (gray rectangle). (B) Alternatively, in a model in which strain in the upper and lower crust is decoupled, regions of low- and high-magnitude extension in the upper crust, as shown in panel A, are smoothed out by variable pure-shear stretching in the lower crust. This schematic strain partitioning can restore back to the inferred Mesozoic crustal thickness. The logic discussed in this figure is similar to that in the "two-layer stretching" model of Gans (1987), but notable differences are discussed in the text. Purple dashed lines are marker horizons that stylistically show relative tilt and extension magnitude. Blue arrows in the middle to lower crust show domains of greater and lesser stretch.

(e.g., Gilbert, 2012). Across this area, there are three domains of alternating low- (10%–15%; domains a and c in Fig. 10) and high-magnitude (>180%; domain b in Fig. 10) extension. Domain a includes the Carson Range and Pine Nut Mountains. Extension magnitudes in the Carson Range are enigmatic due to sparse tilt markers within the uplifted Sierra Nevada granite, but Miocene-to-present fault geometries and basins prohibit extremely high magnitudes of extension. Long (2019) estimated 11% extension across the Carson Range. In the Pine Nut Mountains, ~14% extension has been documented (Long, 2019; this study; Fig. 8). Domain b includes the Singatse and Wassuk Ranges, which have extended >150% (Dilles and Gans, 1995; Surpless et al., 2002; Long, 2019). Finally, domain c includes the Gillis Range, which accommodates significant right-lateral shear in the Walker Lane (e.g., Faulds and Henry, 2008; Lee et al., 2020) on approximately four northwest-striking right-slip faults. Long (2019) constructed a cross section across this region based on mapping by Hardyman (1980) and estimated ~4.9 km of extension (13% extensional strain) (Figs. 1 and 10). Lee et al. (2020)

documented ~32 km of right-lateral offset across the Gillis Range and adjacent Gabbs Valley, which we do not consider in this calculation.

With the knowledge of one-dimensional horizontal strain, ε_h (positive values are extensional strain), we can take the present-day crustal thickness, assume vertically coherent pure-shear deformation, and estimate the pre-extensional crustal thickness using the following relationship:

$$T_i = T_f s_h, \quad (1)$$

where T_i is the initial, pre-extension thickness, T_f is the final thickness, and s_h is the horizontal stretch, $\varepsilon_h + 1$. Restoration to the pre-extension crustal thickness leads to highly variable crustal thickness estimates that are significantly too thick or thin compared to our expectations of ~60-km-thick crust in the Mesozoic (Fig. 10A). The step-function geometry is also unreasonable given modern observations of thickened crust (e.g., Ryan et al., 2016). However, bulk pure-shear restoration of ~58% leads to reasonable pre-extension thickness values (Fig. 10A).

This simple exercise demonstrates that high and low strain in the upper crust must be accommodated via strain compensation at depth, so that the entire crustal section extends nearly uniformly to match vertically uniform horizontal velocity boundary conditions. This proposal is similar to the "two-layer stretching" model of Gans (1987) but does not suggest 6–7 km mafic underplating to balance domains of greater extension and thinning nor entirely uniform stretching of the middle to lower crust. Instead, we argue that middle to lower crust stretching varies to accommodate variable upper-crustal strain, which may be thought of as crustal-scale necking (e.g., Smith, 1978; Smith and Bruhn, 1984; Hauge et al., 1987). A consequence of this is that the upper and lower crust must be decoupled, and extensional strain must be transferred between these layers via ductile shear zone(s) (e.g., Wang et al., 2011). These inferred strain-transfer ductile shear zones may be exhumed as metamorphic core complexes, as observed in the eastern Great Basin (e.g., Miller et al., 1983). For strain compatibility and mass balance, the kinematics of these shear zones depends on relative strain magnitudes of the decoupled upper and lower crust. Here, we assume the Sierra Nevada block translates westward, stretching the Great Basin from a fixed stable North America (Fig. 10B). In domain a, lower strain in the upper crust and greater stretching in the lower crust leads to a top-to-the-east shear zone between the two crustal levels (Fig. 10B), whereas in domain b, the opposite is envisioned, leading to a top-to-the-west shear zone. Domain c is comparable to domain a with top-to-the-east shear (Fig. 10B). This requires either shear-zone separation at the kinematic switches (numbered circles along the mid-crust shear zone in Fig. 10B), small inactive domains, or complex fault stretching (e.g., Means, 1989).

An alternative but related model would suggest the middle- to lower-crustal flow may compensate upper-crustal strain heterogeneities (Block and Royden, 1990; Bird, 1991; Kruse et al., 1991; McKenzie et al., 2000; Schutt et al., 2018). Crustal-flow models are most commonly envisioned to be driven by lateral pressure gradients, and thus for this specific study, crustal material would flow from beneath the low-strain domains (i.e., thicker crust and higher topography) to the higher-strain domains (i.e., thinner crust and lower topography), such as flow from beneath a and c to b in Figure 10B. Flow on the length scales of this study would require viscosities of ~10^{20} Pa·s using established scaling relationships (e.g., Kruse et al., 1991; McQuarrie and Chase, 2000; McKenzie et al., 2000). Schutt et al. (2018) recently estimated lower-crust temperatures in the Great Basin from velocity models of P waves refracted from the crust-mantle boundary (Pn), and inversion assuming power-law lower-crustal rheology yielded viscosities of ≤10^{20} Pa s for wet plagioclase compositions across this studied region. Therefore, crustal flow may be a reasonable mechanism for smoothing topography and Moho geometries. However, we prefer the strain-accommodation model presented in Figure 10B to crustal-flow models for several reasons discussed below.

Crustal flow for smoothing out topography and/or Moho depth involves crustal inflation of the thinner crustal columns, which would predict some vertical motion in the middle to lower crust (e.g., Block and Royden, 1990; McCarthy et al., 1991). Consortium for Continental Reflection Profiling (COCORP) seismic reflection surveys across this study area show only subhorizontal reflectors (e.g., Allmendinger et al., 1987; Surpless et al., 2002). However, if flow-related inflation involves accretion of flowing material into a crustal column, subhorizontal layering could be expected. Similarly, flow would originate from thicker crustal columns and flow toward thinner ones, and in the example presented here, that would be bidirectional flow from domains A and C toward central domain B (Fig. 10B), which complicates the flow geometry, derivations of flow kinematics, and mass balance in each crustal column.

Poiseuille flow requires sustained lateral pressure gradients (e.g., Klemperer, 2006), and thus this process would cease once these gradients are removed, making it hard to envision how this process can remain active during the entire extensional process. Alternatively, basal shear from the lower crust or mantle lithosphere could drive Couette flow, although this process is not commonly invoked in the Great Basin. We acknowledge that crustal-flow mechanisms remain potentially viable to explain the observations in this study but argue that a model of variable middle to lower crust stretching may accommodate differential upper-crustal strain. Channel flow implies that strain accommodation is driven by vertical forces due to lateral pressure gradients, whereas vertically decoupled pure-shear stretching accommodation, as preferred in this study, is controlled by subhorizontal forces related to plate-boundary conditions, which is consistent with our interpretations of plate-boundary stresses modulating the observed two phases of extension. Either case requires substantial decoupling of upper and middle to lower crust kinematics.

It is unclear why certain domains accommodate higher magnitudes of upper-crustal extension that is apparently smoothed out at depth. This may be due to rheologic conditioning and strengthening, such as Mesozoic granitic bodies or Cenozoic middle to lower crust mafic intrusions or underplating, which could selectively strengthen certain crustal domains (e.g., Gans, 1987; Liu and Furlong, 1994). P- to S-wave velocity ratios (V_p/V_s) vary across the

study region, suggesting variable quartz contents (Lowry and Pérez-Gussinyé, 2011), which could lead to heterogeneous rock strength. Alternatively, based on our current understanding, the Singatse and Wassuk Ranges started deforming slightly earlier than the Pine Nut Mountains and Carson Range (e.g., Dilles and Gans, 1995; Surpless et al., 2002; this study), and strain-weakening processes (e.g., Chester et al., 1993) could have worked as a positive feedback to continually focus strain in these older established fault zones. Finally, these differences in upper-crustal extension may reflect necking instabilities during lithospheric extension, which could yield regions of enhanced thinning at characteristic spacings (Fletcher and Hallet, 1983). This model is favored in regions of hot crust with high thermal gradients, which thus may be applicable to the Great Basin (e.g., Miller and Gans, 1989; Surpless et al., 2002; Hyndman, 2019; Zuza et al., 2020a, 2021).

Reconstructions of Pre-Cenozoic Crustal Thickness

We have synthesized extension along an ~150-km-long transect and suggest that crustal thickening or thinning calculations based on documented upper-crustal strain assuming vertically coherent pure-shear deformation may not be valid. That is, high strain observed in the upper crust may not reflect high strain of the entire crustal column. Therefore, using local upper-crust extension estimates to reconstruct paleo–crustal thickness, as commonly done for the Mesozoic Nevadaplano orogenic plateau (e.g., Coney and Harms, 1984; Best et al., 2009; Long, 2019), can lead to overinterpreted, somewhat unjustified thickness estimates and distributions. The classic Coney and Harms (1984) reconstruction assumed vertically coherent pure-shear extension (e.g., England, 1982) and, predictably, inferred thicker crust in western and eastern Nevada where high-strain extensional systems are documented (e.g., around Yerington, the northern Snake Range metamorphic core complex, and the Colorado River extensional corridor). However, here we have argued that continental deformation must have been more variably accommodated and vertically and laterally partitioned. Therefore, we urge caution in using these local range-scale extension estimates, such as from map-view patterns across the Nevadaplano, to elucidate finer-scale variations in paleo–crustal thickness (Fig. 11).

Field-based range-scale extension estimates get incorporated into regional kinematic models (e.g., McQuarrie and Wernicke, 2005), which may be perpetuated in dynamic simulations (Bahadori and Holt, 2019). These inferred orogenic plateau geometries are inconsistent with observations of the analogous present-day Puna-Altiplano (central Andes) (Fig. 11) or Tibetan Plateaus. Specifically, they suggest that the Nevadaplano plateau margins were thicker relative to the plateau center (Fig. 11B). This geometry is at odds with our knowledge of how thickened plateaus and their elevated GPE are supported by stresses across plateau margins (e.g., England and Houseman, 1989; Molnar et al., 1993; Ghosh et al., 2006; England and Molnar, 1997; Rey et al., 2001). A thickening retroarc thrust system would preferentially focus strain in low-GPE regions, if they existed (e.g., Fig. 11B), and therefore this geometry appears improbable. An alternative explanation for this geometry would be lithospheric viscosity variations due to mantle and/or crustal strengthening (e.g., Liu and Furlong, 1994; Xu et al., 2021), but evidence for these variations on spatial scales correlative to those of paleo–crustal thickness maps has not been presented. Furthermore, thinner crust in the middle of the plateau would imply lower topography, which should develop as a

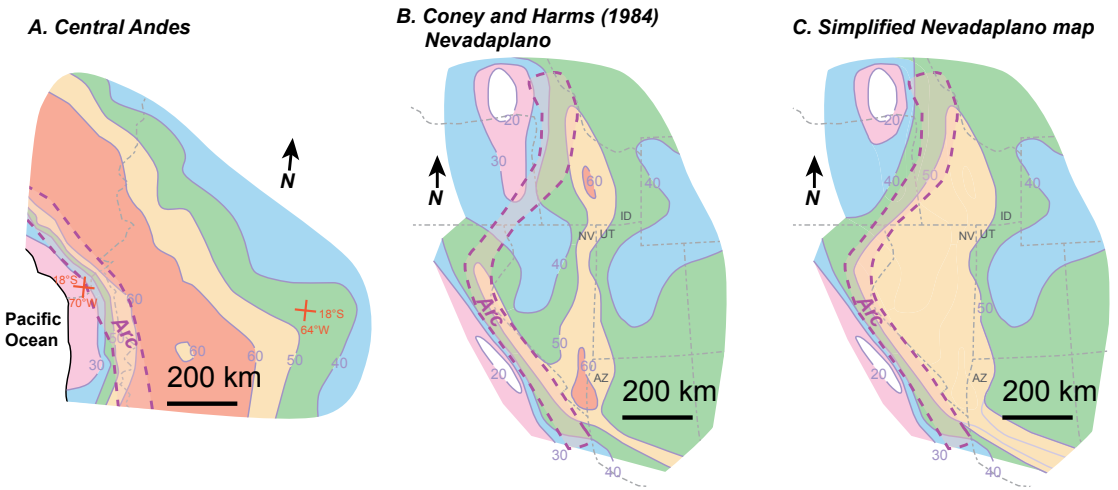

Figure 11. Comparison of crustal thickness between the central Andes and Nevadaplano orogenic plateaus. (A, B) Receiver function–based crustal thickness of (A) the central Andes (modified from Ryan et al., 2016) compared at the same scale with (B) the Nevadaplano reconstruction of Coney and Harms (1984). (C) Schematic Nevadaplano crustal thickness map emphasizing a simpler geometry with a uniform crustal thickness across the central plateau, which is more similar to the analogous Andean plateau in A. Contours in all panels are crustal thickness values in kilometers. Purple dashed polygon shows the ancient and modern arc system. State abbreviations for spatial reference: ID—Idaho; NV—Nevada; UT—Utah.

thick sedimentary basin, such as the ~8–12-km-thick Cenozoic Qaidam Basin in Tibet (e.g., Wang et al., 2021). This is not observed in the Nevadaplano.

Instead, orogen-scale calculations of crustal stretching may provide better first-order estimates of paleo–crustal thickness. For example, Coney and Harms (1984) noted 40% bulk extension across the Basin and Range before their consideration of local extension anomalies. Similarly, the broad data set of Long (2019) implies bulk extension across Nevada of 46%, which would yield a pre-extension crustal thickness of ~54 km. We argue that value, which is comparable that of to other orogenic plateaus and is supported by geochemical proxies (e.g., Chapman et al., 2015) and stable isotope work on paleo-elevation (e.g., Cassel et al., 2014), is probably a reliable estimate within the resolution of field-geology data sets (Fig. 11C). The pre-Miocene topography of this broad plateau has implications for reconstructions of paleoclimate and the impact of topography on atmospheric circulation (e.g., Poage and Chamberlain, 2002; Mulch and Chamberlain, 2018).

CONCLUSIONS

Basin and Range extension has encroached westward against the relatively stable Sierra Nevada block since the Miocene. We investigated this transition zone, which is further overprinted by Walker Lane transtension as part of the Carson domain, via systematic field study of the northern Pine Nut Mountains. We document a conformable section of tilted volcanic strata that span ca. 14.2–6.8 Ma and were erupted as part of the Ancestral Cascade arc. We interpret that Basin and Range extension initiated in this region after the youngest conformable unit, post–6.8 Ma, which is consistent with other studies. Restoration of a balanced cross section suggests 14% extension across the Pine Nut Mountains at an extensional rate of ~0.4 mm yr^{-1}. Our results confirm two phases of extension in the transition zone ca. 15–14 Ma and post–6.8 Ma, with relative tectonic quiescence between these intervals. We interpret this pulsed deformation to reflect dynamic plate-boundary conditions driving extension, which does not support models that rely on built-up GPE to drive plateau collapse.

Walker Lane transtension initiated after ca. 6.8 Ma. Related structures include a possible left-slip segment of the Bull Canyon fault, which parallels other northeast-striking faults in the Carson domain of the Walker Lane, and recently active (Middle to Late Pleistocene) north-striking faults with dip-slip to oblique right-slip normal kinematics that probably accommodate active shear in the Walker Lane.

Integrating this study with nearby constraints for extension reveals heterogeneous extensional strain (i.e., <15% to >150%) in the western Basin and Range, from the Carson Range in the west to the Gillis Range in the east. We argue that these extreme extension variations could not have been uniformly affecting the vertical crustal column via pure-shear deformation because the implied pre-extensional thickness geometries or the present-day Moho depths would also vary significantly. All evidence suggests relatively smooth Moho horizons across this transect. We posit that strain is accommodated differently at decoupled crustal levels to result in smooth homogenous crustal thickness values despite the significantly heterogeneous extensional evolution. Strain is efficiently partitioned vertically, driven by vertically uniform plate-boundary conditions. This case study across an ~150-km-long transect demonstrates that the use of upper-crust extension estimates assuming pure shear, as commonly done for the Mesozoic Nevadaplano orogenic plateau, may not reliably constrain pre-extension crustal thickness.

ACKNOWLEDGMENTS

This research was supported by the U.S. National Earthquake Hazards Reduction Program (G18AP00082) and National Science Foundation (EAR 1830139). The views and conclusions contained in this document are those of the authors and should not be interpreted as representing the opinions or policies of the U.S. Geological Survey. Mention of trade names or commercial products does not constitute their endorsement by the U.S. Geological Survey. Additional support was provided by the Nevada Petroleum and Geothermal Society and the Robert D. Hatcher Research Award from the Geological Society of America. Matt Heizler is thanked for guidance and help with argon analyses at New Mexico Tech. We appreciate formal reviews by an anonymous reviewer and Joseph Colgan, and editorial handling and constructive comments by Associate Editor Todd LaMaskin and Science Editor Shanaka de Silva.

REFERENCES CITED

Adams, K.D., and Wesnousky, S.G., 1998, Shoreline processes and the age of the Lake Lahontan highstand in the Jessup embayment, Nevada: Geological Society of America Bulletin, v. 110, p. 1318–1332, https://doi.org/10.1130/0016-7606(1998)110<1318:SPATAO>2.3.CO;2.

Allmendinger, R.W., Brewer, J.A., Brown, L.D., Kaufman, S., Oliver, J.E., and Houston, R.S., 1982, COCORP profiling across the Rocky Mountain Front in southern Wyoming, Part 2: Precambrian basement structure and its influence on Laramide deformation: Geological Society of America Bulletin, v. 93, p. 1253–1263, https://doi.org/10.1130/0016-7606(1982)93<1253:CPATRM>2.0.CO;2.

Allmendinger, R.W., Sharp, J.W., Von Tish, D., Serpa, L., Brown, L., Kaufman, S., Oliver, J., and Smith, R.B., 1983, Cenozoic and Mesozoic structure of the eastern Basin and Range province, Utah, from COCORP seismic-reflection data: Geology, v. 11, p. 532–536, https://doi.org/10.1130/0091-7613(1983)11<532:CAMSOT>2.0.CO;2.

Allmendinger, R.W., Hauge, T.A., Hauser, E.C., Potter, C.J., Klemperer, S.L., Nelson, K.D., Knuepfer, P., and Oliver, J., 1987, Overview of the COCORP 40°N transect, western United States: The fabric of an orogenic belt: Geological Society of America Bulletin, v. 98, p. 308–319, https://doi.org/10.1130/0016-7606(1987)98<308:OOTCNT>2.0.CO;2.

Atwater, T., 1970, Implications of plate tectonics for the Cenozoic tectonic evolution of western North America: Geological Society of America Bulletin, v. 81, p. 3513–3536, https://doi.org/10.1130/0016-7606(1970)81[3513:IOPTFT]2.0.CO;2.

Atwater, T., and Stock, J., 1998, Pacific–North America plate tectonics of the Neogene southwestern United States: An update: International Geology Review, v. 40, p. 375–402, https://doi.org/10.1080/00206819809465216.

Avouac, J.-P., and Tapponnier, P., 1993, Kinematic model of active deformation in central Asia: Geophysical Research Letters, v. 20, p. 895–898, https://doi.org/10.1029/93GL00128.

Bahadori, A., and Holt, W.E., 2019, Geodynamic evolution of southwestern North America since the Late Eocene: Nature Communications, v. 10, 5213, https://doi.org/10.1038/s41467-019-12950-8.

Beck, S.L., Zandt, G., Myers, S.C., Wallace, T.C., Silver, P.G., and Drake, L., 1996, Crustal-thickness variations in the central Andes: Geology, v. 24, p. 407–410, https://doi.org/10.1130/0091-7613(1996)024<0407:CTVITC>2.3.CO;2.

Bennett, R.A., Wernicke, B.P., Niemi, N.A., Friedrich, A.M., and Davis, J.L., 2003, Contemporary strain rates in the northern Basin and Range province from GPS data: Tectonics, v. 22, 1008, https://doi.org/10.1029/2001TC001355.

Best, M.G., Christiansen, E.H., and Blank, R.H., Jr., 1989, Oligocene caldera complex and calc-alkaline tuffs and lavas of the Indian Peak volcanic field, Nevada and Utah: Geological Society of America Bulletin, v. 101, p. 1076–1090, https://doi.org/10.1130/0016-7606(1989)101<1076:OCCACA>2.3.CO;2.

Best, M.G., Barr, D.L., Christiansen, E.H., Gromme, S., Deino, A.L., and Tingey, D.G., 2009, The Great Basin Altiplano during the middle Cenozoic ignimbrite flareup: Insights

from volcanic rocks: International Geology Review, v. 51, p. 589–633, https://doi.org/10.1080/00206810902867690.
Best, M.G., Christiansen, E.H., and Gromme, S., 2013, Introduction: The 36–18 Ma southern Great Basin, USA, ignimbrite province and flareup: Swarms of subduction-related supervolcanoes: Geosphere, v. 9, p. 260–274, https://doi.org/10.1130/GES00870.1.
Bird, P., 1991, Lateral extrusion of lower crust from under high topography in the isostatic limit: Journal of Geophysical Research, v. 96, p. 10,275–10,286, https://doi.org/10.1029/91JB00370.
Block, L., and Royden, L.H., 1990, Core complex geometries and regional scale flow in the lower crust: Tectonics, v. 9, p. 557–567, https://doi.org/10.1029/TC009i004p00557.
Bormann, J.M., Hammond, W.C., Kreemer, C., and Blewitt, G., 2016, Accommodation of missing shear strain in the Central Walker Lane, western North America: Constraints from dense GPS measurements: Earth and Planetary Science Letters, v. 440, p. 169–177, https://doi.org/10.1016/j.epsl.2016.01.015.
Busby, C.J., 2013, Birth of a plate boundary at ca. 12 Ma in the Ancestral Cascades arc, Walker Lane belt of California and Nevada: Geosphere, v. 9, p. 1147–1160, https://doi.org/10.1130/GES00928.1.
Cao, W., and Paterson, S., 2016, A mass balance and isostasy model: Exploring the interplay between magmatism, deformation and surface erosion in continental arcs using central Sierra Nevada as a case study: Geochemistry Geophysics Geosystems, v. 17, p. 2194–2212, https://doi.org/10.1002/2015GC006229.
Cashman, P.H., and Fontaine, S.A., 2000, Strain partitioning in the northern Walker Lane, western Nevada and northeastern California: Tectonophysics, v. 326, p. 111–130, https://doi.org/10.1016/S0040-1951(00)00149-9.
Cashman, P.H., Trexler, J.H., Muntean, T.W., Faulds, J.E., Louie, J.N., and Oppliger, G.L., 2009, Neogene evolution of the Sierra Nevada–Basin and Range transition zone at the latitude of Carson City, Nevada, *in* Oldow, J.S., and Cashman, P.H., eds., Late Cenozoic Structure and Evolution of the Great Basin–Sierra Nevada Transition: Geological Society of America Special Paper 447, p. 171–188, https://doi.org/10.1130/2009.2447(10).
Cassata, W.S., Renne, P.R., and Shuster, D.L., 2009, Argon diffusion in plagioclase and implications for thermochronometry: A case study from the Bushveld Complex, South Africa: Geochimica et Cosmochimica Acta, v. 73, p. 6600–6612, https://doi.org/10.1016/j.gca.2009.07.017.
Cassel, E.J., Graham, S.A., and Chamberlain, C.P., 2009, Cenozoic tectonic and topographic evolution of the northern Sierra Nevada, California, through stable isotope paleoaltimetry in volcanic glass: Geology, v. 37, p. 547–550, https://doi.org/10.1130/G25572A.1.
Cassel, E.J., Breecker, D.O., Henry, C.D., Larson, T.E., and Stockli, D.F., 2014, Profile of a paleo-orogen: High topography across the present-day Basin and Range from 40 to 23 Ma: Geology, v. 42, p. 1007–1010, https://doi.org/10.1130/G35924.1.
Castor, S.B., 1972, Geology of the central Pine Nut and northern Buckskin Ranges, Nevada: A study of Mesozoic intrusive activity [Ph.D. thesis]: Reno, University of Nevada, 290 p.
Chapman, J.B., Ducea, M.N., DeCelles, P.G., and Profeta, L., 2015, Tracking changes in crustal thickness during orogenic evolution with Sr/Y: An example from the North American Cordillera: Geology, v. 43, p. 919–922, https://doi.org/10.1130/G36996.1.
Chester, F.M., Evans, J.P., and Biegel, R.L., 1993, Internal structure and weakening mechanisms of the San Andreas fault: Journal of Geophysical Research, v. 98, p. 771–786, https://doi.org/10.1029/92JB01866.
Christiansen, R.L., Yeats, R.S., Graham, S.A., Niem, W.A., Niem, A.R., and Snavely, P.D., Jr., 1992, Post-Laramide geology of the U.S. Cordilleran region, *in* Burchfiel, B.C., Lipman, P.W., and Zoback, M.L., eds., The Cordilleran Orogen: Conterminous U.S.: Boulder, Colorado, Geological Society of America, The Geology of North America, v. G-3, p. 261–406, https://doi.org/10.1130/DNAG-GNA-G3.261.
Colgan, J.P., and Henry, C.D., 2009, Rapid middle Miocene collapse of the Mesozoic orogenic plateau in north-central Nevada: International Geology Review, v. 51, p. 920–961, https://doi.org/10.1080/00206810903056731.
Colgan, J.P., John, D.A., Henry, C.D., and Fleck, R.J., 2008, Large-magnitude Miocene extension of the Eocene Caetano caldera, Shoshone and Toiyabe Ranges, Nevada: Geosphere, v. 4, p. 107–130, https://doi.org/10.1130/GES00115.1.
Colgan, J.P., Johnstone, S.A., and Shuster, D.L., 2020, Timing of Cenozoic extension in the southern Stillwater Range and Dixie Valley, Nevada: Tectonics, v. 39, e2019TC005757, https://doi.org/10.1029/2019TC005757.
Coney, P.J., and Harms, T.A., 1984, Cordilleran metamorphic core complexes: Cenozoic extensional relics of Mesozoic compression: Geology, v. 12, p. 550–554, https://doi.org/10.1130/0091-7613(1984)12<550:CMCCCE>2.0.CO;2.
Coney, P.J., and Reynolds, S.J., 1977, Cordilleran Benioff zones: Nature, v. 270, p. 403–406, https://doi.org/10.1038/270403a0.
Cousens, B., Prytulak, J., Henry, C., Alcazar, A., and Brownrigg, T., 2008, Geology, geochronology, and geochemistry of the Miocene–Pliocene Ancestral Cascades arc, northern Sierra Nevada, California and Nevada: The roles of the upper mantle, subducting slab, and the Sierra Nevada lithosphere: Geosphere, v. 4, p. 829–853, https://doi.org/10.1130/GES00166.1.
Davis, G.A., and Burchfiel, B.C., 1973, Garlock fault: An intracontinental transform structure, southern California: Geological Society of America Bulletin, v. 84, p. 1407–1422, https://doi.org/10.1130/0016-7606(1973)84<1407:GFAITS>2.0.CO;2.
DeCelles, P.G., 2004, Late Jurassic to Eocene evolution of the Cordilleran thrust belt and foreland basin system, western USA: American Journal of Science, v. 304, p. 105–168, https://doi.org/10.2475/ajs.304.2.105.
DeCelles, P.G., and Graham, S.A., 2015, Cyclical processes in the North American Cordilleran orogenic system: Geology, v. 43, p. 499–502, https://doi.org/10.1130/G36482.1.
DeMets, C., and Merkouriev, S., 2016, High-resolution reconstructions of Pacific–North America plate motion: 20 Ma to present: Geophysical Journal International, v. 207, p. 741–773, https://doi.org/10.1093/gji/ggw305.
Dickinson, W.R., 2004, Evolution of the North American cordillera: Annual Review of Earth and Planetary Sciences, v. 32, p. 13–45, https://doi.org/10.1146/annurev.earth.32.101802.120257.
Dickinson, W.R., 2006, Geotectonic evolution of the Great Basin: Geosphere, v. 2, p. 353–368, https://doi.org/10.1130/GES00054.1.
Dickinson, W.R., and Snyder, W.S., 1978, Plate tectonics of the Laramide orogeny, *in* Matthews, V., III, ed., Laramide Folding Associated with Basement Block Faulting in the Western United States: Geological Society of America Memoir 151, p. 355–366, https://doi.org/10.1130/MEM151-p355.
Dilles, J.H., and Gans, P.B., 1995, The chronology of Cenozoic volcanism and deformation in the Yerington area, western Basin and Range and Walker Lane: Geological Society of America Bulletin, v. 107, p. 474–486, https://doi.org/10.1130/0016-7606(1995)107<0474:TCOCVA>2.3.CO;2.
Dilles, J.H., and Wright, J.E., 1988, The chronology of early Mesozoic arc magmatism in the Yerington district of western Nevada and its regional implications: Geological Society of America Bulletin, v. 100, p. 644–652, https://doi.org/10.1130/0016-7606(1988)100<0644:TCOEMA>2.3.CO;2.
Dixon, T.H., Miller, M., Farina, F., Wang, H., and Johnson, D., 2000, Present-day motion of the Sierra Nevada block and some tectonic implications for the Basin and Range province, North American Cordillera: Tectonics, v. 19, p. 1–24, https://doi.org/10.1029/1998TC001088.
du Bray, E.A., and John, D.A., 2011, Petrologic, tectonic, and metallogenic evolution of the Ancestral Cascades magmatic arc, Washington, Oregon, and northern California: Geosphere, v. 7, p. 1102–1133, https://doi.org/10.1130/GES00669.1.
England, P., 1982, Some numerical investigations of large scale continental deformation, *in* Hsu, K.J., ed., Mountain Building Processes: New York, Academic Press, p. 129–139.
England, P., and Houseman, G., 1986, Finite strain calculations of continental deformation: 2. Comparison with the India-Asia collision zone: Journal of Geophysical Research, v. 91, p. 3664–3676, https://doi.org/10.1029/JB091iB03p03664.
England, P., and Houseman, G., 1989, Extension during continental convergence, with application to the Tibetan Plateau: Journal of Geophysical Research, v. 94, p. 17,561–17,579, https://doi.org/10.1029/JB094iB12p17561.
England, P., and Molnar, P., 1997, Active deformation of Asia: From kinematics to dynamics: Science, v. 278, p. 647–650, https://doi.org/10.1126/science.278.5338.647.
Ernst, W.G., 2010, Young convergent-margin orogens, climate, and crustal thickness—A Late Cretaceous–Paleogene Nevadaplano in the American Southwest?: Lithosphere, v. 2, p. 67–75, https://doi.org/10.1130/L84.1.
Evans, E.L., Thatcher, W.R., Pollitz, F.F., and Murray, J.R., 2016, Persistent slip rate discrepancies in the eastern California (USA) shear zone: Geology, v. 44, p. 691–694, https://doi.org/10.1130/G37967.1.
Faulds, J.E., and Henry, C.D., 2008, Tectonic influences on the spatial and temporal evolution of the Walker Lane: An incipient transform fault along the evolving Pacific–North American plate boundary, *in* Spencer, J.E., and Titley, S.R., eds., Ores and Orogenesis: Circum-Pacific Tectonics, Geologic Evolution, and Ore Deposits: Arizona Geological Society Digest 22, p. 437–470.
Faulds, J.E., Henry, C.D., and Hinz, N.H., 2005, Kinematics of the northern Walker Lane: An incipient transform fault along the Pacific–North American plate boundary: Geology, v. 33, p. 505–508, https://doi.org/10.1130/G21274.1.
Flesch, L.M., Holt, W.E., Haines, A.J., and Shen-Tu, B., 2000, Dynamics of the Pacific–North American plate boundary in the western United States: Science, v. 287, p. 834–836, https://doi.org/10.1126/science.287.5454.834.

Fletcher, R.C., and Hallet, B., 1983, Unstable extension of the lithosphere: A mechanical model for basin-and-range structure: Journal of Geophysical Research, v. 88, p. 7457–7466, https://doi.org/10.1029/JB088iB09p07457.

Gans, P.B., 1987, An open-system, two-layer crustal stretching model for the eastern Great Basin: Tectonics, v. 6, p. 1–12, https://doi.org/10.1029/TC006i001p00001.

Ghosh, A., Holt, W.E., Flesch, L.M., and Haines, A.J., 2006, Gravitational potential energy of the Tibetan Plateau and the forces driving the Indian plate: Geology, v. 34, p. 321–324, https://doi.org/10.1130/G22071.1.

Gilbert, H., 2012, Crustal structure and signatures of recent tectonism as influenced by ancient terranes in the western United States: Geosphere, v. 8, p. 141–157, https://doi.org/10.1130/GES00720.1.

Gleadow, A.J.W., Belton, D.X., Kohn, B.P., and Brown, R.W., 2002, Fission track dating of phosphate minerals and the thermochronology of apatite: Reviews in Mineralogy and Geochemistry, v. 48, p. 579–630, https://doi.org/10.2138/rmg.2002.48.16.

Hammond, W.C., and Thatcher, W., 2004, Contemporary tectonic deformation of the Basin and Range province, western United States: 10 years of observation with the Global Positioning System: Journal of Geophysical Research. Solid Earth, v. 109, B08403, https://doi.org/10.1029/2003JB002746.

Hammond, W.C., Kreemer, C., and Blewitt, G., 2009, Geodetic constraints on contemporary deformation in the northern Walker Lane: 3. Central Nevada seismic belt postseismic relaxation, *in* Oldow, J.S., and Cashman, P.H., eds., Late Cenozoic Structure and Evolution of the Great Basin–Sierra Nevada Transition: Geological Society of America Special Paper 447, p. 33–54, https://doi.org/10.1130/2009.2447(03).

Haproff, P.J., Zuza, A.V., and Yin, A., 2018, West-directed thrusting south of the eastern Himalayan syntaxis indicates clockwise crustal flow at the indenter corner during the India-Asia collision: Tectonophysics, v. 722, p. 277–285, https://doi.org/10.1016/j.tecto.2017.11.001.

Hardyman, R.F., 1980, Geologic map of the Gillis Canyon quadrangle, Mineral County, Nevada: U.S. Geological Survey Miscellaneous Investigations Series Map I-1237, 1 sheet, scale 1:48,000.

Harrison, T.M., 1982, Diffusion of ^{40}Ar in hornblende: Contributions to Mineralogy and Petrology, v. 78, p. 324–331, https://doi.org/10.1007/BF00398927.

Hauge, T.A., Allmendinger, R.W., Caruso, C., Hauser, E.C., Klemperer, S.L., Opdyke, S., Potter, C.J., Sanford, W., Brown, L., Kaufman, S., and Oliver, J., 1987, Crustal structure of western Nevada from COCORP deep seismic-reflection data: Geological Society of America Bulletin, v. 98, p. 320–329, https://doi.org/10.1130/0016-7606(1987)98<320:CSOWNF>2.0.CO;2.

Henry, C.D., 2008, Ash-flow tuffs and paleovalleys in northeastern Nevada: Implications for Eocene paleogeography and extension in the Sevier hinterland, northern Great Basin: Geosphere, v. 4, p. 1–35, https://doi.org/10.1130/GES00122.1.

Henry, C.D., and Faulds, J.E., 2010, Ash-flow tuffs in the Nine Hill, Nevada, paleovalley and implications for tectonism and volcanism of the western Great Basin, USA: Geosphere, v. 6, p. 339–369, https://doi.org/10.1130/GES00548.1.

Henry, C.D., and John, D.A., 2013, Magmatism, ash-flow tuffs, and calderas of the ignimbrite flareup in the western Nevada volcanic field, Great Basin, USA: Geosphere, v. 9, p. 951–1008, https://doi.org/10.1130/GES00867.1.

Henry, C.D., and Perkins, M.E., 2001, Sierra Nevada–Basin and Range transition near Reno, Nevada: Two-stage development at 12 and 3 Ma: Geology, v. 29, p. 719–722, https://doi.org/10.1130/0091-7613(2001)029<0719:SNBART>2.0.CO;2.

Henry, C.D., McGrew, A.J., Colgan, J.P., Snoke, A.W., Brueseke, M.E., Lee, J., and Evans, J.P., 2011, Timing, distribution, amount, and style of Cenozoic extension in the northern Great Basin, *in* Lee, J., and Evans, J.P., eds., Geologic Field Trips to the Basin and Range, Rocky Mountains, Snake River Plain, and Terranes of the US Cordillera: Geological Society of America Field Guide 21, p. 27–66, https://doi.org/10.1130/2011.0021(02).

Henry, C.D., Hinz, N.H., Faulds, J.E., Colgan, J.P., John, D.A., Brooks, E.R., Cassel, E.J., Garside, L.J., Davis, D.A., and Castor, S.B., 2012, Eocene–Early Miocene paleotopography of the Sierra Nevada–Great Basin–Nevadaplano based on widespread ash-flow tuffs and paleovalleys: Geosphere, v. 8, p. 1–27, https://doi.org/10.1130/GES00727.1.

Henry, C.D., Castor, S.B., Starkel, W.A., Ellis, B.S., Wolff, J.A., Laravie, J.A., McIntosh, W.C., and Heizler, M.T., 2017, Geology and evolution of the McDermitt caldera, northern Nevada and southeastern Oregon, western USA: Geosphere, v. 13, p. 1066–1112, https://doi.org/10.1130/GES01454.1.

Humphreys, E., Hessler, E., Dueker, K., Farmer, G.L., Erslev, E., and Atwater, T., 2003, How Laramide-age hydration of North American lithosphere by the Farallon slab controlled subsequent activity in the western United States: International Geology Review, v. 45, p. 575–595, https://doi.org/10.2747/0020-6814.45.7.575.

Hyndman, R.D., 2019, Mountain building orogeny in precollision hot backarcs: North American Cordillera, India-Tibet, and Grenville Province: Journal of Geophysical Research: Solid Earth, v. 124, p. 2057–2079, https://doi.org/10.1029/2018JB016697.

Ketcham, R.A., Carter, A., Donelick, R.A., Barbarand, J., and Hurford, A.J., 2007, Improved modeling of fission-track annealing in apatite: American Mineralogist, v. 92, p. 799–810, https://doi.org/10.2138/am.2007.2281.

Klemperer, S.L., 2006, Crustal flow in Tibet: Geophysical evidence for the physical state of Tibetan lithosphere, and inferred patterns of active flow, *in* Law, R.D., Searle, M.P., and Godin, L., eds., Channel Flow, Ductile Extrusion and Exhumation in Continental Collision Zones: Geological Society of London Special Publication 268, p. 39–70, https://doi.org/10.1144/GSL.SP.2006.268.01.03.

Kreemer, C., Blewitt, G., and Hammond, W.C., 2009, Geodetic constraints on contemporary deformation in the northern Walker Lane: 2. Velocity and strain rate tensor analysis, *in* Oldow, J.S., and Cashman, P.H., eds., Late Cenozoic Structure and Evolution of the Great Basin–Sierra Nevada Transition: Geological Society of America Special Paper 447, p. 17–31, https://doi.org/10.1130/2009.2447(02).

Kreemer, C., Hammond, W.C., Blewitt, G., Holland, A.A., and Bennet, R.A., 2012, A geodetic strain rate model for the Pacific–North American plate boundary, western United States: Nevada Bureau of Mines and Geology Map 178, scale 1:5,000,000 at latitude 39°N.

Kruse, S., McNutt, M., Phipps-Morgan, J., Royden, L., and Wernicke, B., 1991, Lithospheric extension near Lake Mead, Nevada: A model for ductile flow in the lower crust: Journal of Geophysical Research, v. 96, p. 4435–4456, https://doi.org/10.1029/90JB02621.

Lee, J., Hoxey, A.K.R., Calvert, A., and Dubyoski, P., 2020, Plate boundary trench retreat and dextral shear drive intracontinental fault-slip histories: Neogene dextral faulting across the Gabbs Valley and Gillis Ranges, Central Walker Lane, Nevada: Geosphere, v. 16, p. 1249–1275, https://doi.org/10.1130/GES02240.1.

Levy, D.A., Zuza, A.V., Haproff, P.J., and Odlum, M.L., 2021, Early Permian tectonic evolution of the Last Chance thrust system: An example of induced subduction initiation along a plate boundary transform: Geological Society of America Bulletin, v. 133, p. 1105–1127, https://doi.org/10.1130/B35752.1.

Li, X., Huang, W., Pierce, I.K.D., Angster, S.J., and Wesnousky, S.G., 2017, Characterizing the Quaternary expression of active faulting along the Olinghouse, Carson, and Wabuska lineaments of the Walker Lane: Geosphere, v. 13, p. 2119–2136, https://doi.org/10.1130/GES01483.1.

Liu, M., and Furlong, K.P., 1994, Intrusion and underplating of mafic magmas: Thermal-rheological effects and implications for Tertiary tectonomagmatism in the North American Cordillera: Tectonophysics, v. 237, p. 175–187, https://doi.org/10.1016/0040-1951(94)90253-4.

Long, S.P., 2019, Geometry and magnitude of extension in the Basin and Range Province (39°N), Utah, Nevada, and California, USA: Constraints from a province-scale cross section: Geological Society of America Bulletin, v. 131, p. 99–119, https://doi.org/10.1130/B31974.1.

Lowry, A.R., and Pérez-Gussinyé, M., 2011, The role of crustal quartz in controlling Cordilleran deformation: Nature, v. 471, p. 353–357, https://doi.org/10.1038/nature09912.

Luyendyk, B.P., Kamerling, M.J., and Terres, R., 1980, Geometric model for Neogene crustal rotations in southern California: Geological Society of America Bulletin, v. 91, p. 211–217, https://doi.org/10.1130/0016-7606(1980)91<211:GMFNCR>2.0.CO;2.

McCarthy, J., Larkin, S.P., Fuis, G.S., Simpson, R.W., and Howard, K.A., 1991, Anatomy of a metamorphic core complex: Seismic refraction/wide-angle reflection profiling in southeastern California and western Arizona: Journal of Geophysical Research, v. 96, p. 12,259–12,291, https://doi.org/10.1029/91JB01004.

McDougall, I., and Harrison, T.M., 1999, Geochronology and Thermochronology by the ^{40}Ar/^{39}Ar Method: Oxford, UK, Oxford University Press, 269 p.

McIntosh, W.C., Heizler, M., Peters, L., and Esser, R., 2003, ^{40}Ar/^{39}Ar geochronology at the New Mexico Bureau of Geology and Mineral Resources: New Mexico Bureau of Geology and Mineral Resources Open File Report OF-AR-1, 7 p.

McKenzie, D., and Jackson, J., 1983, The relationship between strain rates, crustal thickening, palaeomagnetism, finite strain and fault movements within a deforming zone: Earth and Planetary Science Letters, v. 65, p. 182–202, https://doi.org/10.1016/0012-821X(83)90198-X.

McKenzie, D., Nimmo, F., Jackson, J.A., Gans, P.B., and Miller, E.L., 2000, Characteristics and consequences of flow in the lower crust: Journal of Geophysical Research, v. 105, p. 11,029–11,046, https://doi.org/10.1029/1999JB900446.

McQuarrie, N., and Chase, C.G., 2000, Raising the Colorado Plateau: Geology, v. 28, p. 91–94, https://doi.org/10.1130/0091-7613(2000)028<0091:RTCP>2.0.CO;2.

McQuarrie, N., and Wernicke, B.P., 2005, An animated tectonic reconstruction of southwestern North America since 36 Ma: Geosphere, v. 1, p. 147–172, https://doi.org/10.1130/GES00016.1.
Meade, B.J., 2007, Present-day kinematics at the India-Asia collision zone: Geology, v. 35, p. 81–84, https://doi.org/10.1130/G22924A.1.
Meade, B.J., and Hager, B.H., 2005, Block models of crustal motion in southern California constrained by GPS measurements: Journal of Geophysical Research, v. 110, B03403, https://doi.org/10.1029/2004JB003209.
Means, W.D., 1989, Stretching faults: Geology, v. 17, p. 893–896, https://doi.org/10.1130/0091-7613(1989)017<0893:SF>2.3.CO;2.
Miller, D.M., and Hoisch, T.D., 1995, Jurassic tectonics of northeastern Nevada and northwestern Utah from the perspective of barometric studies, *in* Miller, D.M„ and Busby, C., eds., Jurassic Magmatism and Tectonics of the North American Cordillera: Geological Society of America Special Paper 299, p. 267–294, https://doi.org/10.1130/SPE299-p267.
Miller, E.L., and Gans, P.B., 1989, Cretaceous crustal structure and metamorphism in the hinterland of the Sevier thrust belt, western U.S. Cordillera: Geology, v. 17, p. 59–62, https://doi.org/10.1130/0091-7613(1989)017<0059:CCSAMI>2.3.CO;2.
Miller, E.L., Gans, P.B., and Garing, J., 1983, The Snake Range décollement: An exhumed mid-Tertiary ductile-brittle transition: Tectonics, v. 2, p. 239–263, https://doi.org/10.1029/TC002i003p00239.
Molnar, P., and Tapponnier, P., 1975, Cenozoic tectonics of Asia: Effects of a continental collision: Science, v. 189, p. 419–426, https://doi.org/10.1126/science.189.4201.419.
Molnar, P., England, P., and Martinod, J., 1993, Mantle dynamics, uplift of the Tibetan Plateau, and the Indian monsoon: Reviews of Geophysics, v. 31, p. 357–396, https://doi.org/10.1029/93RG02030.
Moore, J.G., and Archbold, N.L., 1969, Geology and mineral deposits of Lyon, Douglas, and Ormsby Counties, Nevada: Nevada Bureau of Mines and Geology Bulletin 75, 45 p.
Mulch, A., Chamberlain, C.P., Hoorn, C., Perrigo, A., and Antonelli, A., 2018, Stable isotope paleoaltimetry: Paleotopography as a key element in the evolution of landscapes and life, *in* Hoorn, C., Perrigo, A., and Antonelli, A., eds., Mountains, Climate and Biodiversity: Wiley Blackwell, p. 81–93.
Muntean, T.W., 2001, Evolution and stratigraphy of the Neogene Sunrise Pass Formation of the Gardnerville sedimentary basin, Douglas County, Nevada [M.S. thesis]: Reno, University of Nevada, 306 p.
Nagorsen-Rinke, S., Lee, J., and Calvert, A., 2013, Pliocene sinistral slip across the Adobe Hills, eastern California–western Nevada: Kinematics of fault slip transfer across the Mina deflection: Geosphere, v. 9, p. 37–53, https://doi.org/10.1130/GES00825.1.
Nicholson, C., Sorlien, C.C., Atwater, T., Crowell, J.C., and Luyendyk, B.P., 1994, Microplate capture, rotation of the western Transverse Ranges, and initiation of the San Andreas transform as a low-angle fault system: Geology, v. 22, p. 491–495, https://doi.org/10.1130/0091-7613(1994)022%3C0491:MCROTW%3E2.3.CO;2.
Noble, D.C., 1962, Mesozoic geology of the southern Pine Nut Range, Douglas County, Nevada [Ph.D. thesis]: Stanford, California, Stanford University, 200 p.
Oldow, J.S., Kohler, G., and Donelick, R.A., 1994, Late Cenozoic extensional transfer in the Walker Lane strike-slip belt, Nevada: Geology, v. 22, p. 637–640, https://doi.org/10.1130/0091-7613(1994)022<0637:LCETIT>2.3.CO;2.
Pearce, J.A., 2008, Geochemical fingerprinting of oceanic basalts with applications to ophiolite classification and the search for Archean oceanic crust: Lithos, v. 100, p. 14–48, https://doi.org/10.1016/j.lithos.2007.06.016.
Pearce, J.A., and Peate, D.W., 1995, Tectonic implications of the composition of volcanic arc magmas: Annual Review of Earth and Planetary Sciences, v. 23, p. 251–285, https://doi.org/10.1146/annurev.ea.23.050195.001343.
Pierce, I.K., Wesnousky, S.G., Owen, L.A., Bormann, J.M., Li, X., and Caffee, M., 2021, Accommodation of plate motion in an incipient strike-slip system: The Central Walker Lane: Tectonics, v. 40, e2019TC005612, https://doi.org/10.1029/2019TC005612.
Platt, J.P., and Becker, T.W., 2010, Where is the real transform boundary in California?: Geochemistry Geophysics Geosystems, v. 11, Q06012, https://doi.org/10.1029/2010GC003060.
Platt, J.P., and Becker, T.W., 2013, Kinematics of rotating panels of E-W faults in the San Andreas system: What can we tell from geodesy?: Geophysical Journal International, v. 194, p. 1295–1301, https://doi.org/10.1093/gji/ggt189.
Poage, M.A., and Chamberlain, C.P., 2002, Stable isotopic evidence for a pre-Middle Miocene rain shadow in the western Basin and Range: Implications for the paleotopography of the Sierra Nevada: Tectonics, v. 21, no. 4, https://doi.org/10.1029/2001TC001303.
Profeta, L., Ducea, M.N., Chapman, J.B., Paterson, S.R., Gonzales, S.M.H., Kirsch, M., Petrescu, L., and DeCelles, P.G., 2015, Quantifying crustal thickness over time in magmatic arcs: Scientific Reports, v. 5, 17786, https://doi.org/10.1038/srep17786.
Proffett, J.M., Jr., 1977, Cenozoic geology of the Yerington district, Nevada, and implications for the nature and origin of Basin and Range faulting: Geological Society of America Bulletin, v. 88, p. 247–266, https://doi.org/10.1130/0016-7606(1977)88<247:CGOTYD>2.0.CO;2.
Proffett, J.M., Jr., and Dilles, J.H., 1984, Geologic map of the Yerington district, Nevada: Nevada Bureau of Mines and Geology Map 77, scale 1:24,000.
Rey, P., Vanderhaeghe, O., and Teyssier, C., 2001, Gravitational collapse of the continental crust: Definition, regimes and modes: Tectonophysics, v. 342, p. 435–449, https://doi.org/10.1016/S0040-1951(01)00174-3.
Ridley, J., 2013, Ore Deposit Geology: Cambridge, UK, Cambridge University Press, 398 p., https://doi.org/10.1017/CBO9781139135528.
Russell, K., 1981, Geology and ore deposits of the Como mining district, Lyon County, Nevada [M.S. thesis]: Fresno, California State University, 85 p.
Ryan, J., Beck, S., Zandt, G., Wagner, L., Minaya, E., and Tavera, H., 2016, Central Andean crustal structure from receiver function analysis: Tectonophysics, v. 682, p. 120–133, https://doi.org/10.1016/j.tecto.2016.04.048.
Ryan, W.B.F., Carbotte, S.M., Coplan, J., O'Hara, S., Melkonian, A., Arko, R., Weissel, R.A., Ferrini, V., Goodwillie, A., Nitsche, F., Bonczkowski, J., and Zemsky, R., 2009, Global Multi-Resolution Topography (GMRT) synthesis data set: Geochemistry, Geophysics, Geosystems, v. 10, https://doi.org/10.1029/2008GC002332.
Saleeby, J., Dunne, G., Anderson, T.H., Didenko, A.N., Johnson, C.L., Khanchuk, A.I., and MacDonald, J.H., 2015, Temporal and tectonic relations of early Mesozoic arc magmatism, southern Sierra Nevada, California, *in* Anderson, T.H., Didenko, A.N., Johnson, C.L., Khanchuk, A.I., and MacDonald, J.H., Jr., eds., Late Jurassic Margin of Laurasia—A Record of Faulting Accommodating Plate Rotation: Geological Society of America Special Paper 513, p. 223–268, https://doi.org/10.1130/2015.2513(05).
Say, M.C., and Zuza, A.V., 2020, Late Miocene transition between Basin and Range extension and Walker Lane tectonics, northern Pine Nut Mountains, Nevada: New insights from geologic mapping and $^{40}Ar/^{39}Ar$ geochronology, *in* Koutz, F.R., and Pennell, W.M., eds., Geological Society of Nevada Symposium 2020, p. 1351–1374.
Schutt, D.L., Lowry, A.R., and Buehler, J.S., 2018, Moho temperature and mobility of lower crust in the western United States: Geology, v. 46, p. 219–222, https://doi.org/10.1130/G39507.1.
Schweickert, R.A., 1978, Triassic and Jurassic paleogeography of the Sierra Nevada and adjacent regions, California and western Nevada, *in* Howell, D.G., and McDougall, K.A., eds., Mesozoic Paleogeography of the Western United States: Los Angeles, Society of Economic Paleontologists and Mineralogists, Pacific Section, Pacific Coast Paleogeography Symposium 2, p. 361–384.
Smith, R.B., 1978, Seismicity, crustal structure, and intraplate tectonics of the interior of the western Cordillera, *in* Smith, R.B., and Eaton, G.P., Cenozoic Tectonics and Regional Geophysics of the Western Cordillera: Geological Society of America Memoir 152, p. 111–144, https://doi.org/10.1130/MEM152-p111.
Smith, R.B., and Bruhn, R.L., 1984, Intraplate extensional tectonics of the Eastern Basin-Range: Inferences on structural style from seismic reflection data, regional tectonics, and thermal-mechanical models of brittle-ductile deformation: Journal of Geophysical Research, v. 89, p. 5733–5762, https://doi.org/10.1029/JB089iB07p05733.
Sonder, L.J., and Jones, C.H., 1999, Western United States extension: How the west was widened: Annual Review of Earth and Planetary Sciences, v. 27, p. 417–462, https://doi.org/10.1146/annurev.earth.27.1.417.
Stewart, J.H., 1988, Tectonics of the Walker Lane belt, western Great Basin: Mesozoic and Cenozoic deformation in a zone of shear, *in* Ernst, W.G., ed., Metamorphism and Crustal Evolution of the Western United States: Englewood Cliffs, New Jersey, Prentice Hall, p. 681–713.
Stewart, J.H., 1997, Triassic and Jurassic stratigraphy and paleontology of west-central Nevada and eastern California: U.S. Geological Survey Open-File Report 97-495, 37 p.
Stewart, J.H., 1999, Geologic map of the Carson City 30 × 60 minute quadrangle, Nevada: Nevada Bureau of Mines and Geology Map 118, scale 1;100,000.
Stock, J.M., and Lee, J., 1994, Do microplates in subduction zones leave a geological record?: Tectonics, v. 13, p. 1472–1487, https://doi.org/10.1029/94TC01808.
Stockli, D.F., 1999, Regional timing and spatial distribution of Miocene extension in the northern Basin and Range province [Ph.D. thesis]: Stanford, California, Stanford University, 239 p.
Stockli, D.F., Surpless, B.E., Dumitru, T.A., and Farley, K.A., 2002, Thermochronological constraints on the timing and magnitude of Miocene and Pliocene extension in the central

Wassuk Range, western Nevada: Tectonics, v. 21, no. 4, https://doi.org/10.1029/2001TC001295.

Sturmer, D.M., and Faulds, J.E., 2018, Kinematic evolution of the Olinghouse fault and the role of a major sinistral fault in the Walker Lane dextral shear zone, Nevada, USA: Journal of Structural Geology, v. 115, p. 47–63, https://doi.org/10.1016/j.jsg.2018.07.006.

Surpless, B.E., Stockli, D.F., Dumitru, T.A., and Miller, E.L., 2002, Two-phase westward encroachment of Basin and Range extension into the northern Sierra Nevada: Tectonics, v. 21, no. 1, https://doi.org/10.1029/2000TC001257.

Svarc, J.L., Savage, J.C., Prescott, W.H., and Ramelli, A.R., 2002, Strain accumulation and rotation in western Nevada, 1993–2000: Journal of Geophysical Research, v. 107, no. B5, https://doi.org/10.1029/2001JB000579.

Tapponnier, P., Peltzer, G., Le Dain, A.Y., Armijo, R., and Cobbold, P., 1982, Propagating extrusion tectonics in Asia: New insights from simple experiments with plasticine: Geology, v. 10, p. 611–616, https://doi.org/10.1130/0091-7613(1982)10<611:PETIAN>2.0.CO;2.

Thatcher, W., 1995, Microplate versus continuum descriptions of active tectonic deformation: Journal of Geophysical Research, v. 100, p. 3885–3894, https://doi.org/10.1029/94JB03064.

Thatcher, W., Foulger, G.R., Julian, B.R., Svarc, J., Quilty, E., and Bawden, G.W., 1999, Present-day deformation across the Basin and Range province, western United States: Science, v. 283, p. 1714–1718, https://doi.org/10.1126/science.283.5408.1714.

Timmermans, A.C., Cousens, B.L., and Henry, C.D., 2020, Geochemical study of Cenozoic mafic volcanism in the west-central Great Basin, western Nevada, and the Ancestral Cascades Arc, California: Geosphere, v. 16, p. 1179–1207, https://doi.org/10.1130/GES01535.1.

Trexler, J.H., Jr., Cashman, P.H., Henry, C.D., Muntean, T., Schwartz, K., TenBrink, A., Faulds, J.E., Perkins, M., and Kelly, T., 2000, Neogene basins in western Nevada document the tectonic history of the Sierra Nevada–Basin and Range transition zone for the last 12 Ma, *in* Lageson, D.R., Peters, S.G., and Lahren, M.M., eds., Great Basin and Sierra Nevada: Geological Society of America Field Guide 2, p. 97–116, https://doi.org/10.1130/0-8137-0002-7.97.

Trexler, J., Cashman, P., and Cosca, M., 2012, Constraints on the history and topography of the northeastern Sierra Nevada from a Neogene sedimentary basin in the Reno-Verdi area, western Nevada: Geosphere, v. 8, p. 548–561, https://doi.org/10.1130/GES00735.1.

Unruh, J., Humphrey, J., and Barron, A., 2003, Transtensional model for the Sierra Nevada frontal fault system, eastern California: Geology, v. 31, p. 327–330, https://doi.org/10.1130/0091-7613(2003)031<0327:TMFTSN>2.0.CO;2.

Vikre, P.G., and McKee, E.H., 1994, Geology, alteration, and geochronology of the Como District, Lyon County, Nevada: Economic Geology, the Bulletin of the Society of Economic Geologists, v. 89, p. 639–646, https://doi.org/10.2113/gsecongeo.89.3.639.

Wang, C., Gao, R., Yin, A., Wang, H., Zhang, Y., Guo, T., Li, Q., and Li, Y., 2011, A mid-crustal strain-transfer model for continental deformation: A new perspective from high-resolution deep seismic-reflection profiling across NE Tibet: Earth and Planetary Science Letters, v. 306, p. 279–288, https://doi.org/10.1016/j.epsl.2011.04.010.

Wang, L., Cheng, F., Zuza, A.V., Jolivet, M., Liu, Y., Guo, Z., Li, X., and Zhang, C., 2021, Diachronous growth of the northern Tibetan plateau derived from flexural modeling: Geophysical Research Letters, v. 48, e2020GL092346, https://doi.org/10.1029/2020GL092346.

Weldon, R., and Humphreys, E., 1986, A kinematic model of southern California: Tectonics, v. 5, p. 33–48, https://doi.org/10.1029/TC005i001p00033.

Wesnousky, S.G., 2005a, Active faulting in the Walker Lane: Tectonics, v. 24, TC3009, https://doi.org/10.1029/2004TC001645.

Wesnousky, S.G., 2005b, The San Andreas and Walker Lane fault systems, western North America: Transpression, transtension, cumulative slip and the structural evolution of a major transform plate boundary: Journal of Structural Geology, v. 27, p. 1505–1512, https://doi.org/10.1016/j.jsg.2005.01.015.

Wyld, S.J., 2002, Structural evolution of a Mesozoic backarc fold-and-thrust belt in the U.S. Cordillera: New evidence from northern Nevada: Geological Society of America Bulletin, v. 114, p. 1452–1468, https://doi.org/10.1130/0016-7606(2002)114<1452:SEOAMB>2.0.CO;2.

Xu, X., Zuza, A.V., Yin, A., Lin, X., Chen, H., and Yang, S., 2021, Permian plume-strengthened Tarim lithosphere controls the Cenozoic deformation pattern of the Himalayan-Tibetan orogen: Geology, v. 49, p. 96–100, https://doi.org/10.1130/G47961.1.

Yang, H., Moresi, L.N., and Quigley, M., 2020, Fault spacing in continental strike-slip shear zones: Earth and Planetary Science Letters, v. 530, 115906, https://doi.org/10.1016/j.epsl.2019.115906.

Yin, A., 2010, Cenozoic tectonic evolution of Asia: A preliminary synthesis: Tectonophysics, v. 488, p. 293–325, https://doi.org/10.1016/j.tecto.2009.06.002.

Yin, A., and Taylor, M.H., 2011, Mechanics of V-shaped conjugate strike-slip faults and the corresponding continuum mode of continental deformation: Geological Society of America Bulletin, v. 123, p. 1798–1821, https://doi.org/10.1130/B30159.1.

Yonkee, W.A., and Weil, A.B., 2015, Tectonic evolution of the Sevier and Laramide belts within the North American Cordillera orogenic system: Earth-Science Reviews, v. 150, p. 531–593, https://doi.org/10.1016/j.earscirev.2015.08.001.

Zuza, A.V., and Carlson, C.W., 2018, What can strike-slip fault spacing tell us about the plate boundary of western North America?: Terra Nova, v. 30, p. 105–113, https://doi.org/10.1111/ter.12315.

Zuza, A.V., Yin, A., Lin, J., and Ming, S., 2017, Spacing and strength of active continental strike-slip faults: Earth and Planetary Science Letters, v. 457, p. 49–62, https://doi.org/10.1016/j.epsl.2016.09.041.

Zuza, A.V., Thorman, C.H., Henry, C.D., Levy, D.A., Dee, S., Long, S.P., Sandberg, C.A., and Sognard, E., 2020a, Pulsed Mesozoic deformation in the Cordilleran hinterland and evolution of the Nevadaplano: Insights from the Pequop Mountains, NE Nevada: Lithosphere, v. 2020, 8850336, https://doi.org/10.2113/2020/8850336.

Zuza, A.V., Gavillot, Y., Haproff, P.J., and Wu, C., 2020b, Kinematic evolution of a continental collision: Constraining the Himalayan-Tibetan orogen via bulk strain rates: Tectonophysics, v. 797, 228642, https://doi.org/10.1016/j.tecto.2020.228642.

Zuza, A.V., Levy, D.A., and Mulligan, S.R., 2021, Geologic field evidence for non-lithostatic overpressure recorded in the North American Cordillera hinterland, northeast Nevada: Geoscience Frontiers, https://doi.org/10.1016/j.gsf.2020.10.006 (in press).